Aeroelastic Modeling to Study the Wind-Induced Response of a Self-Supported Lattice Tower

Ziad Azzi¹, Amal Elawady^{1,2}, Peter Irwin², Arindam Gan Chowdhury^{1,2}, and Caesar Abi Shdid³

5 Abstract

1

2

3

4

6

7

8

9

10

11

12

13

14

15

16

17

18

19

20

21

The results from a 1:50 scale aeroelastic model of a self-supported steel lattice tower subjected to simulated hurricane winds are presented. The lattice tower considered is a typical structure that is used as part of a tower-insulator-conductor system for electrical transmission infrastructure. The aeroelastic tests were conducted at the NSF Wall of Wind Experimental Facility (WOW EF) at the Florida International University (FIU). The tower was tested at various wind speeds ranging from 50 m/s to 92 m/s (equivalent full-scale speeds) for varying wind directions. Two system identification (SID) techniques were utilized to evaluate along-wind aerodynamic damping and compare with theoretical estimates. The SID techniques were also utilized to evaluate crosswind aerodynamic damping. A buffeting analysis was conducted to estimate the response of the tower and compare it to measured values at the WOW. Drag and moment coefficients were calculated from the measured responses, and the dynamic amplification factors (DAF) as well as gust effect factors were computed. The analysis required consideration of the variation of the turbulence intensity along the height of the tower in the buffeting analytical equations. The drag coefficients are shown to agree with values proposed in the current standards. However, there might be a need to introduce base moment coefficients in lattice tower design. The resonance contribution is shown to reach a maximum of 18% of the peak response of the tower.

22 Keywords: aeroelastic modeling; transmission tower; Wall of Wind; system identification; aero-

23 dynamic damping; buffeting response; drag coefficient; moment coefficient; dynamic amplifica-

24 tion factors.

¹Department of Civil and Environmental Engineering, Florida International University, Miami, FL, USA.

²Extreme Events Institute of International Hurricane Research Center, Florida International University, Miami, FL, USA.

³Department of Civil Engineering, Lebanese American University, Beirut, Lebanon.

1. <u>Introduction</u>

25

26

27

28

29

30

31

32

33

34

35

36

37

38

39

40

41

42

43

44

45

46

Of primary concern to power utility companies around the world is the safe and economic design of electrical transmission lines and their supporting towers. Such structures can be vulnerable to various types of windstorms, including large scale storms such as hurricanes and localized events such as thunderstorms (Holmes, 2015). This paper focuses on large scale storms in which the atmospheric boundary layer is homogenous along the length of the line. However, some of the findings may also be relevant to local storms. Generally, transmission towers are made of steel lattice sections. Such structures are normally designed to be as lightweight as possible to minimize the cost of carrying the electrical conductors over distances of hundreds of kilometers [(Lin et al., 2011); (Lin et al., 2012)]. Transmission towers are in the class of tall, slender, flexible structures sensitive to wind effects, with very small structural damping. Wind loads normally control the design of these towers and previously recorded wind speeds have been documented to reach values as high as 80 m/s (1-min maximum sustained winds), which is equivalent to Category 5 on the Saffir-Simpson hurricane scale (Kalaga and Yenumula, 2017). Therefore, it is important to study their behavior in strong winds including buffeting responses and the potential for vortex shedding and other causes of vibration [(Badruddin Ahmad et al., 1984); (Hiramatsu and Akagi, 1988); (Lou et al., 2000); (Lou et al., 2009); (Lin et al., 2011); (Lin et al., 2012)]. Wind direction plays an important role in the design of lattice sections due to the aerodynamic properties of the latter such as shielding and projected frontal area (or solidity ratio). Such parameters can greatly vary over small angles of wind direction (Mara et al., 2010). Lattice steel towers are also used to support TV and cellular phone antennas as well as microwave communication dishes. As part of today's expanding communication systems, these types of towers cover almost the entirety of the continental United States [(Bayar, 1986); (Lou et al., 2000); (Carril Jr. et al., 2003)].

Traditional wind design standards for such structures assume an atmospheric boundary layer profile to provide the basis of wind loading [(Savory et al., 2001); (Yang and Zhang, 2016)]. There is a need to evaluate wind-induced resonant dynamic response due to the fact that the tower's lower vibration modes can have low enough natural frequency to be excited by the turbulence in the natural wind (Holmes, 1994). Typically, transmission structures have natural frequencies varying between 0.5 and 4 Hz, depending on classification and shape (ASCE 74, 2010).

In addition to the static effect caused by mean wind speed, the dynamic behavior of a transmission tower is three-dimensional. It occurs in the along-wind, the crosswind, and torsional directions under the fluctuating wind pressure [(Mara et al., 2013); (Liang et al., 2015)]. However, current standards still design for the along-wind response of lattice transmission towers. Moreover, cable structures are vulnerable to galloping effects, especially when they are located in cold regions where ice accretion might develop. This effect might modify the conductors' cross-sectional shape so that it becomes aerodynamically and aeroelastically unstable, severely affecting the behavior of the transmission tower (Chabart and Lilien, 1998). Other vulnerabilities of cable structures could be due to vortex shedding excitation, wake interference, and buffeting due to wind gust among others [(Tokoro et al., 2000); (Bartoli et al., 2006)].

The failure of a transmission tower carrying electrical lines can be crucial since it leads to disruption of electrical services. Such disruption has negative economic and social consequences (Shehata and El Damatty, 2008). Boudreaux (1962) first reported damages caused by Hurricane Carla in 1961 to the Houston Lighting & Power Company, which were approximated at about

\$1.5 million at that time. In Japan, Shichiri (1971) documented numerous damages observed in hundreds of transmission towers due to typhoons. In 2018, Hurricane Michael wreaked havoc on several transmission lines and toppled an estimated 100 lattice towers in Florida. The devastation from this Category 5 hurricane with wind speeds reaching 70 m/s was estimated at around \$25 billion [(NOAA, 2019); (FEMA, 2020)]. Observed failure modes of lattice transmission towers reported in existing literature are: (i) buckling of the compression members, (ii) uplift failure of a tension footing, (iii) buckling of a face member, and (iv) horizontal shear failure of the tower [(Dempsey and White, 1996); (Shehata and El Damatty, 2008)]. Hence, it is crucial to investigate the wind-induced response of lattice towers in order to improve their resiliency as stand-alone structures and as part of transmission line systems.

Several numerical, experimental, and field studies have been performed to assess the behavior of transmission towers and lines. Because of the complexity of transmission line systems, numerical models have been difficult to verify, whereas both wind tunnel testing and full-scale measurements are particularly challenging [(Loredo-Souza and Davenport, 2001); (Loredo-Souza, 2014)]. With regards to wind tunnel testing, three different types are being utilized: static, dynamic, and aeroelastic. In static testing, mean aerodynamic forces can be collected from force balances and force (drag and lift) coefficients can then be obtained, whereas in dynamic testing, a two-dimensional section modeling method can be used. In aeroelastic testing, the model replicates, at small scale, the motions of the structure which allows motion dependent aerodynamic effects, such as aerodynamic stiffness and damping, to be included. Such modeling technique comes with many advantages such as better simulation of turbulence effects, reproduction of adjacent topographical features as well as the incorporation of the influence of mode shapes and their interaction. However, it also presents serious challenges such as achieving all required val-

ues of aeroelastic scaling parameters, discussed later on in Table 1 [(Irwin, 1992); (Loredo-Souza and Davenport, 2001); (Loredo-Souza, 2014)].

93

94

95

96

97

98

99

100

101

102

103

104

105

106

107

108

109

110

111

112

113

114

Previous studies on individual lattice towers have focused on field observations, numerical analysis, and finite element computer models to investigate the wind-induced response on such structures [(Badruddin Ahmad et al., 1984); (Holmes, 1996a, 1996b); (Savory et al., 2001); (Choi and Hidayat, 2002); (Lou et al., 2009); (Chen et al., 2014); (Yang and Zhang, 2016)]. The majority of previous aeroelastic testing of transmission towers investigated the behavior and the buffeting response of the whole transmission tower-conductor system [(Lin et al., 2011); (Lin et al., 2012); (Loredo Souza, 2014); (Liang et al., 2015); (Aboshosha et al., 2016); (Elawady et al., 2016a)]. To date, very little research has focused on the wind-induced behavior of tall lattice steel towers or sections using aeroelastic models [(Lou et al., 2000); (Mara el al., 2010)]. Lou et al. (2000) were the first to test an aeroelastic model of a tall steel lattice tower at a length scale of 1:100. They reported that a substantial part of the tower response is buffeting at the fundamental natural frequency of the model. In addition, they also observed that the response of a lattice tower in the two principal sway directions is approximately the same, emphasizing the need to include crosswind vibrations in the design standards, which currently deal with the along-wind response only. Mara et al. (2010) investigated the aerodynamic forces on two 1:10 models of vertical steel lattice towers as well as guyed ones. The models were rotated about two axes and the behavior was recorded for different pitch and yaw angles. The study concluded that the most severe forces occur when the most frontal area of the structure is subjected to wind. It was also emphasized that current standards do not consider the wind-induced forces coming from simultaneous directions, i.e., along-wind and crosswind. Last but not least, international standards do

not adequately consider the crosswind vibration of the lattice towers and the relevant aerodynamic damping.

This study aims to fill the existing gap in the literature and advance the knowledge in lattice structure response. This would be achieved by conducting aeroelastic tests on a complete self-supported lattice tower constructed using a relatively large length scale of 1:50. The following sections describe the design, modeling, and construction of the lattice tower, along with their validation. The along-wind and crosswind aerodynamic damping coefficients are then obtained from acceleration time histories using an iterative approach and subsequently, compared with analytical values. The crosswind response, neglected in all design standards around the world, could prove to affect the resiliency of such structures. The wind-induced buffeting response of the model is then investigated. This includes resonant effects pertaining to the structure's natural frequency and turbulent fluctuations in the oncoming wind. Finally, force and moment coefficients along with dynamic amplification factors are calculated using the data collected from the model and are compared with similar parameters specified in different design standards utilized around the world.

2. <u>Experimental Setup, Design and Validation of the Lattice Tower Model</u>

2.1 Wall of Wind Experimental Facility (WOW EF)

The experiments of this project were carried out at the National Science Foundation (NSF) Natural Hazards Engineering Research Infrastructure (NHERI) Wall of Wind Experimental Facility (WOW EF). The WOW EF utilizes a powerful 12-fan system with the latter organized in two curved rows of six fans each, capable of wind speeds reaching up to 70 m/s. Turbulence characteristics for terrain exposures are achieved using a set of adjustable triangular spires and roughness elements located inside a flow management box upwind of the test section.

The test section, designated as open jet, is 4.3 m high by 6 m wide (Feng et al., 2020). The turntable, on which specimens are erected and rotated to allow testing at different wind directions, has a diameter of 4.9 m. The characteristics of the WOW EF enable testing of a wide range of model scales, and model types including buildings, tower components and appurtenances of such structures (Azzi et al., 2020a, 2020d). Fig. 1a and 1b show the intake side of the WOW EF and the flow management box, respectively. More details on the design and validation of the WOW EF is presented in Chowdhury et al. (2017) along with several case studies at different scales.





Fig. 1: Pictures of the WOW EF: (a) 12-fan system captured from the intake side, and (b) flow management box

2.2 Aeroelastic Modeling for Wind Testing

2.2.1 Scaling, Design and Construction

Although lattice towers come in various shapes and designs, such structures are classified by their type. According to ASCE 74 (2010) and ANSI/TIA-222 (2005), three types of towers are well established for electrical transmission, telecommunication, and antenna use. The three types are: (i) poles and guyed masts, (ii) H-frames, and (iii) self-supported latticed towers (shown in Fig. 2). The main difference between all three types is their fundamental frequency. Generally, poles have the smallest natural frequency with a range of 0.5 to 1 Hz, followed by H-frames with a range of 1 to 2 Hz and latticed towers with a range of 2 to 4 Hz.

The lattice tower selected for this study is classified as a steel double circuit vertical self-supported lattice tower typically used in transmission line industry. This particular tower design is located in coastal areas in the state of Texas, along the Gulf of Mexico. The prototype lattice tower has the following full-scale dimensions: a height h of 27.5 m, a rectangular base with length L of 7.6 m, and a width B of 2.7 m. The cross-section of the tower uniformly decreases along its height until it reaches a constant section. Additionally, the tower has three different levels of identical cross-arms at the top. This allows the attachment of six bundles of conductors, with two at each level. Fig. 2a and 2b illustrate the isometric and frontal views of the tower, respectively.

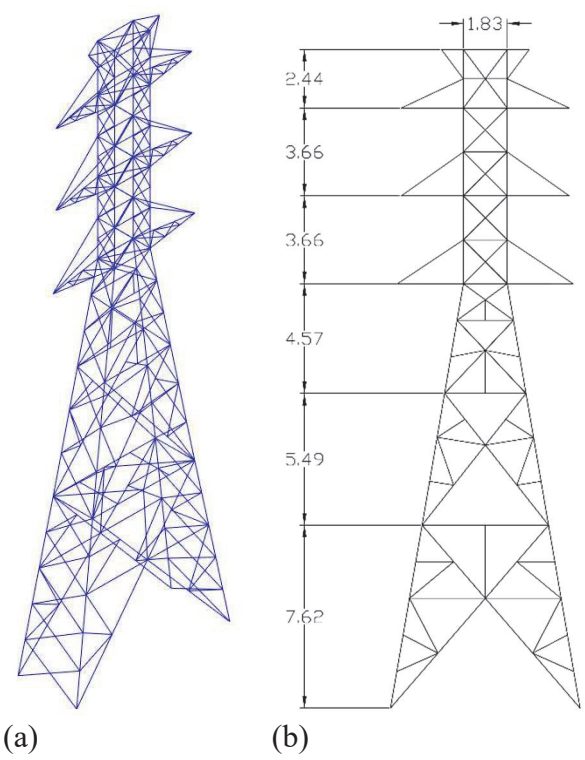


Fig. 2: Steel lattice tower: (a) isometric view, and (b) frontal view (all dimensions in m and at full-scale)

Whenever the geometry and physical properties of a prototype have to be reproduced as a model at smaller scales, care needs to be taken in order to mimic the same dynamic behavior (Azzi, 2016). Normally, it is preferred to use prototype material in the construction of the aeroe-

lastic model to maintain the structural damping, which influences the dynamic responses of the system (Isyumov, 1972). However, since lattice towers are lightweight structures, it is challenging to satisfy the mass scaling using prototype steel material. Therefore, a different metal such as aluminum is usually selected to satisfy the mass scaling requirement [(Elawady et al., 2016a, 2017); (Azzi et al., 2020c)]. Although the structural damping of aluminum is less than that of steel (Mevada and Patel, 2016), the aerodynamic damping for flexible structures such as the lattice tower in this project, tends to be much more dominant than its structural counterpart. Therefore, the discrepancy does not severely impact the results.

For this project, a relatively large length scale λ_L of 1:50 is selected. Froude number Fr is maintained the same on the model as that on the prototype. This means that the ratio between the inertial and gravitational forces is preserved. Some of the other essential parameters required to correctly design the aeroelastic model along with their scaling ratios are summarized in Table 1.

Table 1: Scaling parameters used in the design of the aeroelastic model

Quantity Q	Scaling factor λ_Q	Quantity Q	Scaling factor λ_Q
Length L	1:50	Damping ζ	1:1
Velocity U	$1:50^{1/2}$	Elastic stiffness <i>EI</i>	1:50 ⁵
Mass m	$1:50^3$	Elastic stiffness <i>EA</i>	1:50 ³
Mass moment of inertia I	1:50 ⁵	Force F	1:50 ³
Time t	$1:50^{1/2}$	Bending moment M	1:504
Acceleration a	1:1	Torsional moment T	1:50 ⁴

In building the aeroelastic model, an aluminum hollow spine with a rectangular cross-section of 5.6 mm width by 13.7 mm length was used. The spine had a height of 55 cm (model-scale) and its role was to mimic the structural properties of the vertical part of the tower structure, most importantly, the elastic stiffness *EI*. Although the tower's stiffness is varying along its height, a fixed cross section was used for the spine so as not to violate the elastic stiffness scaling

at any point along the tower height by more than 15%. Note that seven zones were utilized in the design of the tower. The bottom of the spine was embedded inside an aluminum bearing plate of 16 mm thickness. Epoxy was used to glue the spine inside the plate thereby creating a fixity connection. The cross-arms were also designed based on the elastic stiffness EI of their prototype counterparts. Aluminum sheets of 4.6 mm height and 0.51 mm thickness were utilized in the construction and glued to the spine using epoxy. To accurately recreate the tower shape and the wind flow around it, non-structural cladding elements were 3D printed using an ultralight, plastic-like material, and were attached to the spine using thin polystyrene rods. Note that the cladding elements' widths were adjusted to compensate for the addition of the spine and its frontal area. This ensured that the total drag on the tower face, for each zone and in each direction, was appropriately scaled down from the prototype. On another note, the previously mentioned connection between the rods and the cladding elements was conceived so as not to add too much mass nor any additional stiffness to the model. It is worthwhile mentioning that such a design approach using a spine and cladding elements to model the transmission tower has been widely used in the past [(Zhu et al., 2011); (Lin et al., 2011); (Lin et al., 2012); (Hamada, 2014); (Elawady et al., 2016b); (Elawady et al., 2017); (Hamada et al., 2017); (Elawady et al., 2018)]. Moreover, results from experiments conducted on transmission lines with towers designed as a spine complemented with cladding elements have been used in the past to validate numerical models with very good agreement (Elawady et al., 2018). Fig. 3a and 3b show isometric and frontal views of the actual constructed aeroelastic model, respectively.

188

189

190

191

192

193

194

195

196

197

198

199

200

201

202

203

204

205

206

207

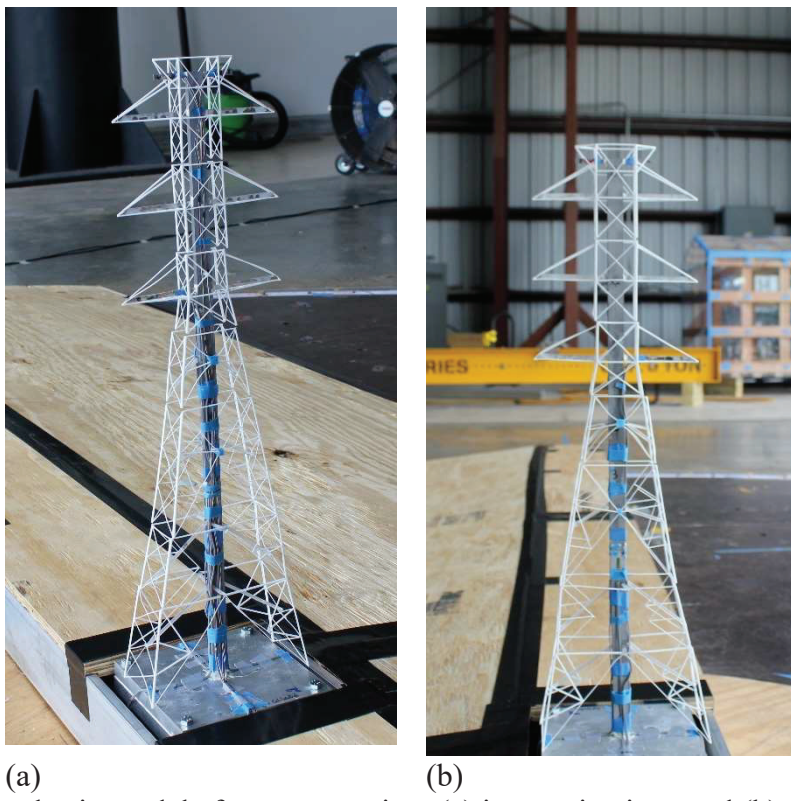


Fig. 3: Aeroelastic model after construction: (a) isometric view, and (b) frontal view

2.2.2 <u>Validation of Dynamic Parameters</u>

In order to validate the design of the aeroelastic model and the different sectional dimensions, properties and materials selected, a replica model was generated on the Finite Element Methods (FEM) software SAP2000 (2020). In the computer simulations, the spine and the crossarms were modeled as rigid frame elements with the former having a fixed restraint at its bottom. The loads introduced by the weight of the non-structural cladding elements were added as gravity point loads at each joint between the elements and the spine. A modal analysis was performed, and the modal deflection shapes were recorded along with their respective frequencies. The obtained frequency values were compared with prototype frequencies, acquired from a modal analysis of the full-scale tower. The results of the modal analysis and the percent difference between the obtained and target model frequencies are summarized in Table 2. Fig. 4a and 4b illustrate the first two modes of vibrations generated by the FEM model. Note that, in Table 2, the target

frequency f_t is equal to the prototype frequency times the relevant scaling factor ($\lambda_f = 7.07$ from Table 1).

Table 2: Summary of modal analysis results

Mode of vibration	Prototype frequency f_p (Hz)	Target frequency f_t (Hz)	FEM-Model frequency f_m (Hz) (design)	Percent difference (%)
Longitudinal	2.25	15.88	15.56	2.02
Transverse	5.10	36.08	35.82	0.72

As can be seen in Table 2, the model frequencies f_m obtained from the modal analysis for both mode shapes closely match the target frequencies f_i . The highest percent difference between the two is around 2%, obtained for mode shape 1. This demonstrates that the choice of materials along with the section dimensions used to generate the aeroelastic model on the FEM software were adequate. The construction and instrumentation of the model as well as the subsequent wind tunnel testing could proceed.

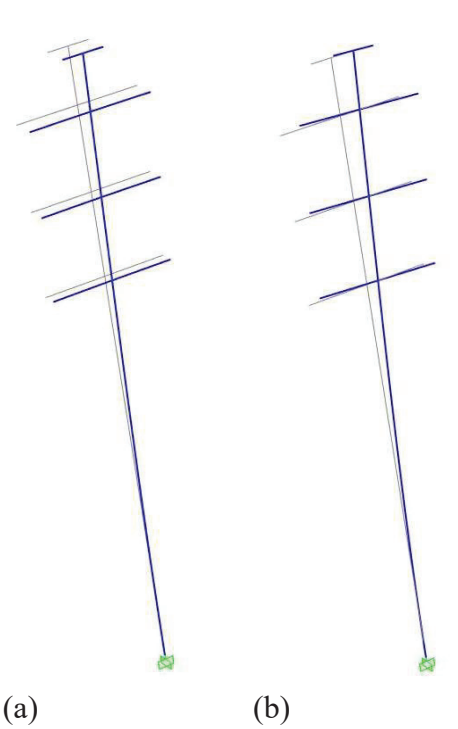


Fig. 4: Mode shapes 1 and 2, respectively: (a) longitudinal vibration (along weak axis), and (b) transverse vibration (along strong axis)

2.3 <u>Instrumentation and Testing Protocol</u>

The tower was instrumented with the following sensors: (i) three 3-axis accelerometers, (ii) one 6-Degrees-Of-Freedom (6-DOF) load cell, and (iii) six strain gauges. Two accelerometers were installed at the top of the tower on the cross-arms, and another was glued at mid-height of the spine. The load cell was fixed at the bottom of the tower in order to capture base shears, base moments, and torsional reactions. Four strain gauges were installed at one third height of the spine with one on each face. The remaining two strain gauges were installed on the bottom cross-arm. The strain gauges were calibrated to allow the measurement of axial forces and moments in the principal directions at their respective point of attachment. Data for the previously described sensors were sampled at 100 Hz. Fig. 5a, 5b and 5c show the location of some of the sensors installed. Finally, two cobra probes were installed at a distance of 4 m behind the model to capture time histories of wind velocities. One probe was installed at mid-height (27.5 cm) and the other probe was installed at tower height (55 cm). Data from the probes were sampled at 2,500 Hz.

Concerning the testing protocol, it was decided to expose the model to four different wind speeds: 7, 9, 11 and 13 m/s at tower height (55 cm, small-scale), representing 49.5, 63.6, 77.8 and 91.9 m/s at prototype height (27.5 m, full-scale). The tower was rotated between 0° and 90° at 15° increments and each angle duration exposure lasted 2 min (about 14 min, full-scale). Note that a wind direction of 0° represents wind along the strong-axis (parallel to the cross-arms) and a wind direction of 90° pertains to wind along the weak-axis of the tower (normal to the cross-arms). The spires and roughness elements depicted in Fig. 1b were adjusted so that the turbulence profile matched that of an equivalent open terrain exposure.

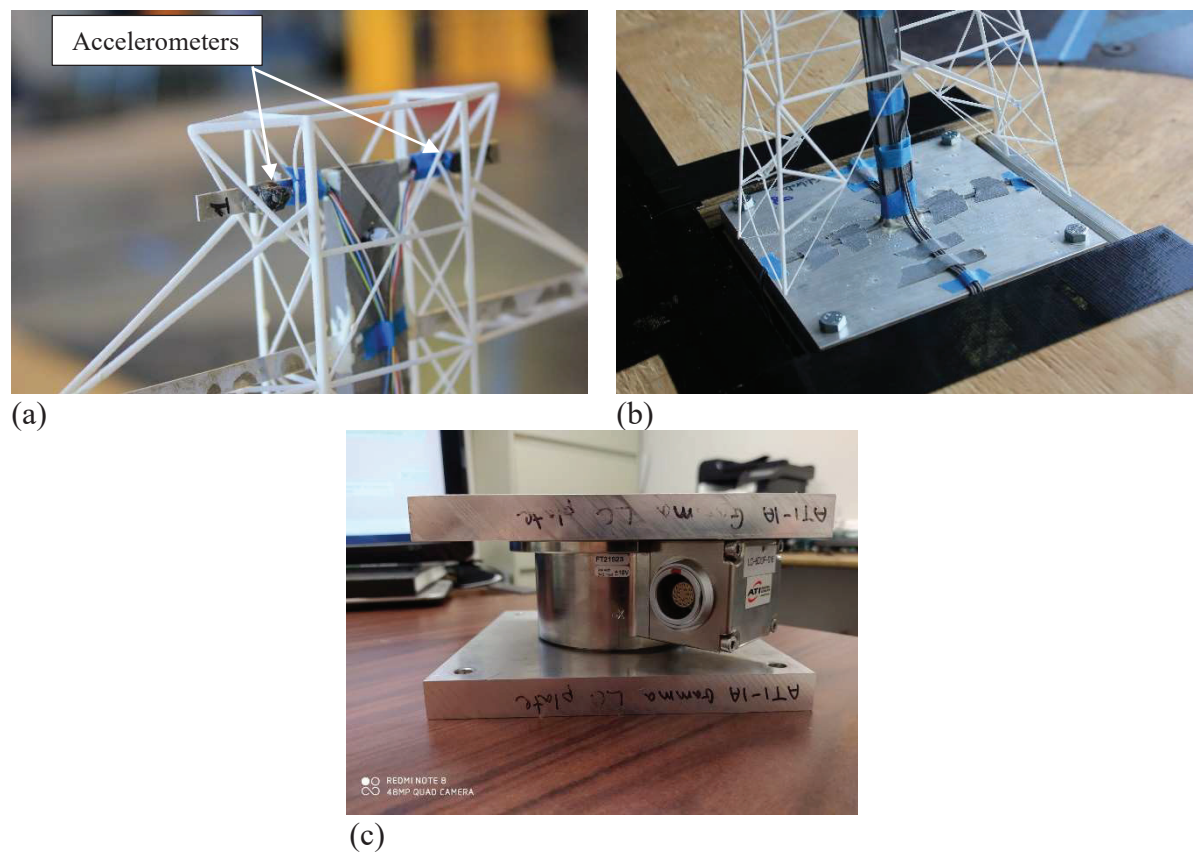


Fig. 5: Location of some of the sensors: (a) two 3-axis accelerometers on top cross-arm, (b) base of tower (load cell is below bearing plate), and (c) 6-DOF load cell used

3. Results and Discussion

This section presents the analysis and discussion of the results obtained from the wind testing of the aeroelastic lattice tower model. First, free vibration tests were conducted on the model in order to verify the mode shapes and their respective frequencies. Second, two system identification (SID) techniques were introduced and applied to the model acceleration data to obtain an estimate of the structural (i.e., no wind applied) and aerodynamic (i.e., wind applied) damping coefficients. Then, experimental damping values were compared with analytical ones in the along-wind direction. An insight into the crosswind aerodynamic damping of the lattice tower is also presented. Third, the buffeting theory is briefly explained, and theoretical RMS accelerations, base shears and moments are compared with experimentally obtained ones. Finally, drag and moment coefficients for the aeroelastic lattice tower are calculated experimentally from

the sensors and compared with standard suggested values. Dynamic amplification factors (DAF) as well as gust effect factors are computed for all recorded parameters, and suggestions as well as recommendations are formulated.

3.1 SID Parameters based on Free Vibration and Damping Estimation

Before the actual wind testing of the tower specimen, a free vibration test was conducted for the purpose of comparing the frequencies of the constructed model with the prototype frequencies. The tower was excited twice: (i) along its strong axis, and (ii) along its weak axis. The excitation consisted of manually pushing the top of the tower in one direction and allowing it to freely oscillate until it went back to its initial position while recording its instantaneous acceleration in that same direction. This verified both mode shapes obtained by the modal analysis of the FEM model (Table 2).

A mechanism was constructed at the WOW using steel supports and electromagnets in order to induce free vibration in the transmission tower by giving it an initial displacement in both strong and weak axes (0° and 90°). A fine string with a negligible mass was attached to the top of the tower in order to displace it by the required amount without altering any of its properties. Note that the displacement was conducted in a way to isolate the mode shape of the tower along its respective direction. Two 3-axis accelerometers were used to record the acceleration time histories at the topmost point of the tower. Fig. 6a and 6b show the mechanism that was devised to conduct the free vibration tests.

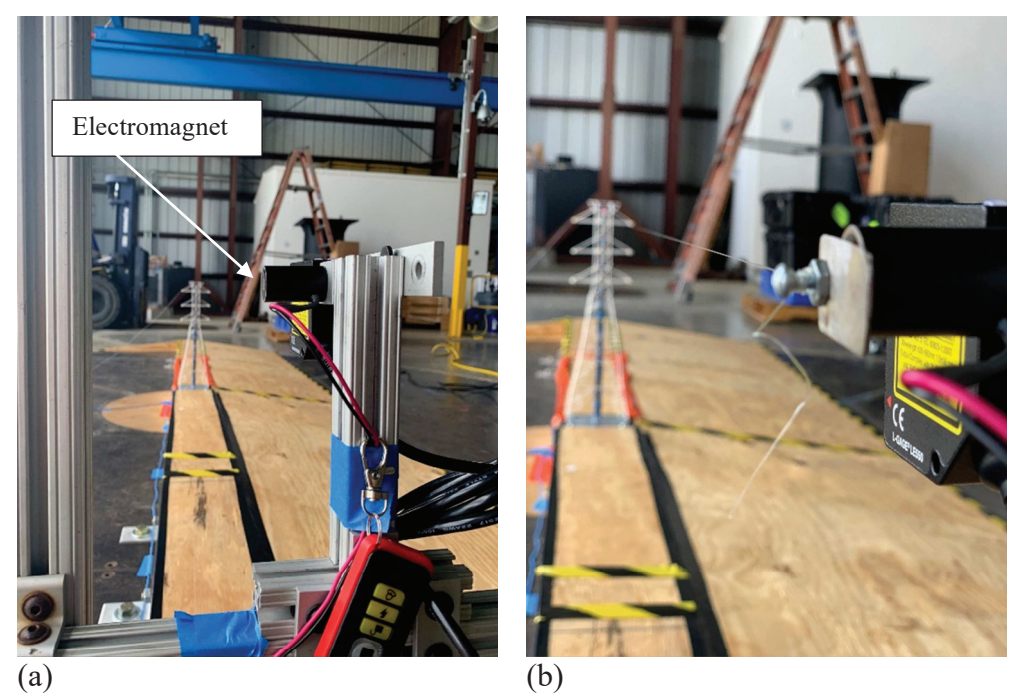


Fig. 6: Mechanism to conduct free vibration tests: (a) electromagnet turned off, and (b) electromagnet turned on (zoomed in picture)

The transmission tower was given an initial displacement of: (i) 0.8 cm along the strong axis, and (ii) 1.5 cm along the weak axis. The initial displacement was measured using a laser displacement transducer, and the electromagnet was turned on whenever the required value was reached. The choice of the initial displacement value was based on the amount of deflection required for the string mechanism to reach the electromagnet location. The electromagnet was then turned off and the structure oscillated freely until reaching its rest position. To assess the structural damping only, i.e., the case of no wind loading, the test was performed twice in order to measure the structural damping ζ_s of the lattice structure for mode shapes 1 and 2. To obtain the aerodynamic damping of the tower, i.e., the case of wind loading, the test was repeated five times (at five different wind speeds) for two separate directions (0° and 90°) and mode shapes 1 and 2, for a total of twenty tests. Accelerations in the x- and y-directions were recorded for each test allowing the capture of the total damping ζ_{tot} (structural + aerodynamic) for the along-wind

and crosswind directions at 0° and 90°. Fig. 7a and 7b show two acceleration time histories of free vibration tests (no wind loading) conducted to excite two separate mode shapes, 1 and 2.

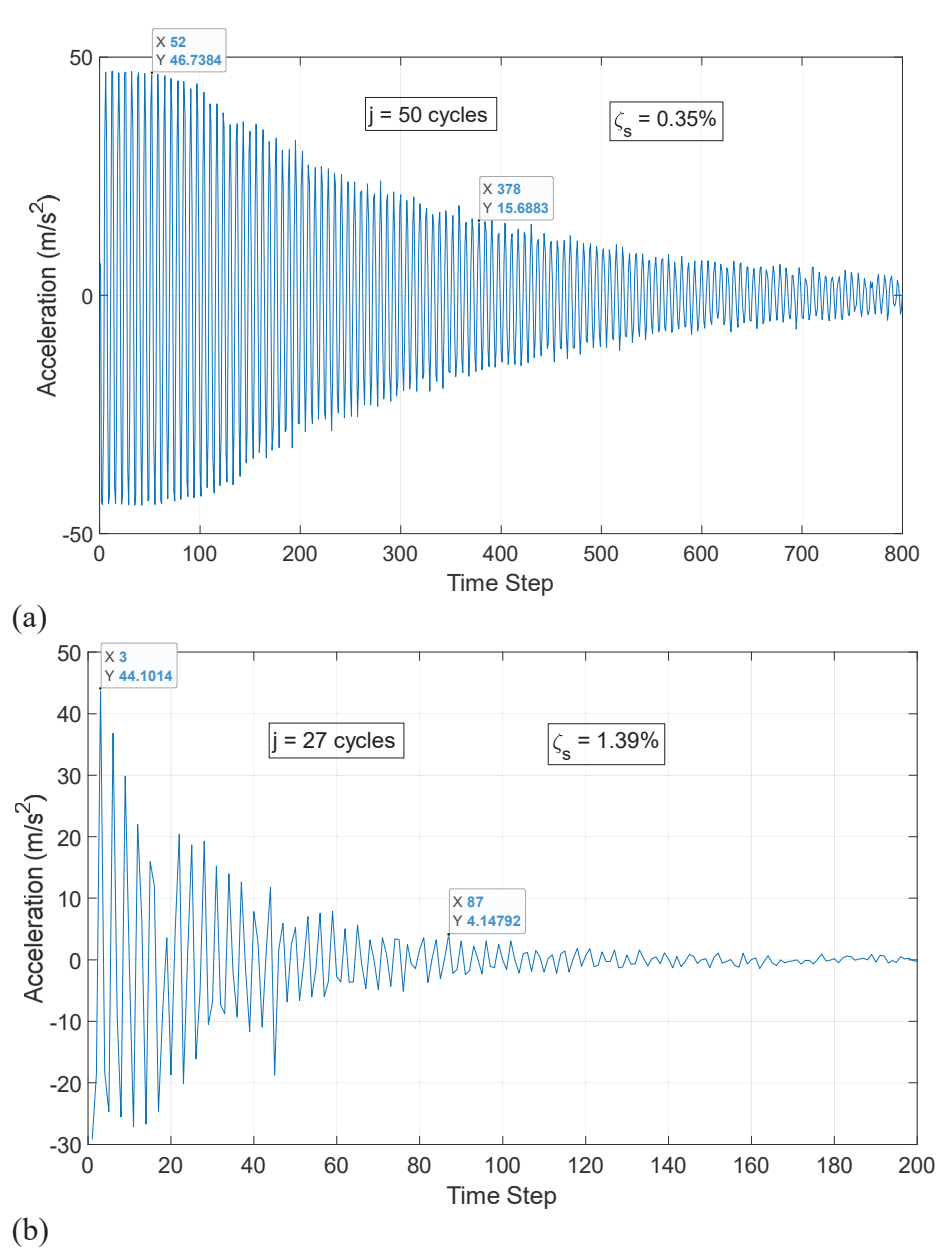


Fig. 7: Acceleration time histories of free vibration tests along: (a) weak axis (mode shape 1), and (b) strong axis (mode shape 2)

From the captured acceleration time histories, the fluctuating response as well as the corresponding frequencies can be obtained using a Fast Fourier Transform (FFT) application. Fig.

8a and 8b illustrate the power spectral densities (PSD) of the acceleration time histories along the weak and strong axes, respectively.

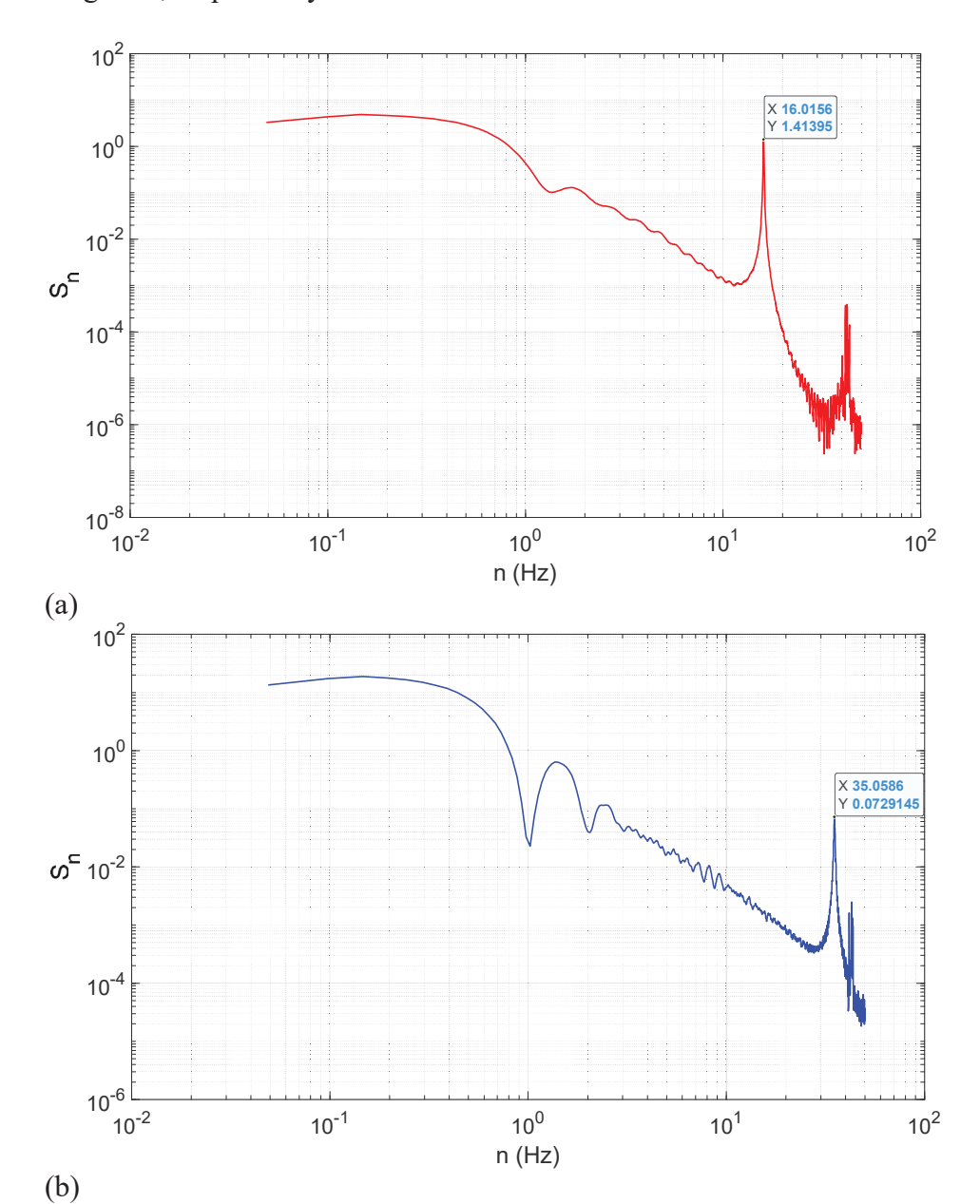


Fig. 8: PSD of acceleration time histories: (a) along weak axis, and (b) along strong axis

By inspecting Fig. 8a and 8b, it can be noted that the frequencies of the fundamental
modes of vibration along weak and strong axes were 16.02 Hz and 35.06 Hz, respectively (seen
in the data boxes). By comparing these values with the target frequencies in Table 2, we obtain a

difference of 0.88% for mode shape 1 and 2.83% for mode shape 2. Such small percent differ-

ences indicate that the construction of the model was adequately representative of its full-scale counterpart during wind tunnel testing.

The self-supported lattice tower can be compared to a single-degree-of-freedom (SDOF) system. For approximation purposes, the system consists of a particle of mass M concentrated at the top of the tower. The tower has a linear elastic behavior and negligible mass with the particle being subjected to an aeroelastic force $F_{ae}(t)$. The displacement at the top of the tower x(t) is opposed by: (i) a restoring force -kx where k is the stiffness of the tower, and (ii) a damping force $-c\dot{x}$ where c is the damping coefficient (Simiu and Yeo, 2019). Eq. 1 shows Newton's second law of motion of the system, which states that the product of the particle's mass M by its acceleration \ddot{x} is equal to the total aeroelastic force applied to the particle above (Azzi, 2016):

$$M.\ddot{x} + c.\dot{x} + k.x = F_{ae}(t) \tag{1}$$

Assigning $n = \sqrt{(k/M)/(2\pi)}$ and $\zeta_{eff} = c/(2\sqrt{(k.M)})$ as the frequency of vibration and the effective damping ratio in the direction of the motion, respectively, Eq. 1 can then be rewritten as Eq. 2 [(Simiu and Yeo, 2019); (Azzi et al., 2020b)]:

$$\ddot{x} + 2\zeta_{eff}.(2\pi.n).\dot{x} + (2\pi.n)^2.x = \frac{F_{ae}(t)}{M}$$
 (2)

In case of free vibration of a SDOF system in one direction, the damping ratio ζ_{eff} becomes the structural damping of the system ζ_s and the term on the right side of Eq. 2 becomes zero since no loading is applied on the structure. Chowdhury and Sarkar (2003, 2004) developed a system identification technique (SID), called the Iterative Least Squares (ILS) approach that allows all eighteen flutter derivatives for a streamlined bridge deck to be obtained from free vibration displacement time histories. In order to obtain the flutter derivatives using the ILS approach, it is necessary to first find the aeroelastically modified effective damping C^{eff} and stiffness K^{eff} matrices, respectively [(Sarkar, 1992); (Sarkar et al., 1994)]. Subsequently, if the free

vibration tests are done twice, once with and once without the WOW fans turned on (i.e., with and without wind loading), then one can obtain the structural and effective damping ratios ζ_s and ζ_{eff} , correspondingly. Hence, the aeroelastic damping ratio ζ_a can be calculated by subtracting ζ_s from ζ_{eff} . More information about the ILS algorithm and its use can be found in Chowdhury and Sarkar (2003, 2004).

In addition to the use of the ILS method, another well-established approach for damping estimation called the Random Decrement (RD) technique [(Jeary, 1986); (Jeary, 1992); (Tamura and Suganuma, 1996); (Takeuchi et al., 2010)] was used. In brief, the RD technique uses a time-domain approach in which the structural responses to operational loads of a certain structure are transformed into random decrement functions. The latter are proportional to the correlation functions of the system operational responses and hence, could be considered as free vibration responses. In this study, values obtained using the two previously mentioned methods are compared to those obtained from the analytical method of obtaining along-wind aerodynamic damping coefficients for lattice towers [(Davenport, 1988); (Loredo-Souza, 1996); (Loredo-Souza and Davenport, 2003)].

Recall that, for the case of no wind loading, the obtained effective damping is none other than the structural ζ_s of the tower. As a check, for both mode shapes 1 and 2, the damping values obtained from the ILS method were compared with the traditional structural damping formula (shown in Eq. 3) established for any typical decay of motion phenomenon [(Strelkov, 1964); (Chopra, 2017)].

$$\zeta_S = \left(\frac{1}{2\pi \cdot j}\right) \cdot \ln\left(\frac{\ddot{x}_1}{\ddot{x}_{j+1}}\right) \tag{3}$$

In Eq. 3, j is the number of cycles selected, \ddot{x}_I and \ddot{x}_{j+I} are the acceleration at time steps 1 and j+I in m/s², respectively.

From Fig. 7a and 7b, the structural damping values for mode shapes 1 and 2, calculated using Eq. 3, are 0.35% and 1.39%, respectively (shown in Fig 7). Note that mode shape 1 pertains to the vibration along the weak axis whereas mode shape 2 is along the strong axis. Using the ILS and RD techniques, the damping values are estimated at 0.37% and 0.39% for mode shape 1 and 1.37% and 1.36% for mode shape 2, respectively. Both experimental techniques are well in agreement for the no wind loading case.

With the WOW fans turned on, Fig. 9a and 9b show the comparison between the same experimental methods and their analytical counterpart. Note that the values presented in the following figures are at the reduced velocity U/(n.B), with U being the wind speed at the top height of the tower in m/s, n being the natural frequency of the tower in the representative mode shape in Hz (i.e., 15.9 Hz in weak axis direction and 35.9 Hz in the strong axis direction) and B being the width of the face of the tower at its mid-height in m (the value of B is 10 cm for the wide face of the tower and 4 cm for the narrow face, at small-scale). The analytical method to calculate the aerodynamic damping of the lattice tower was based on the formula proposed by Loredo-Souza and Davenport (2003), given in Eq. 4:

$$\zeta_{a} = \left(\frac{\rho_{a}}{4\pi \cdot f_{T}}\right) \cdot \left(\frac{\int_{0}^{h} \overline{U}(z) \cdot C_{D}(z) \cdot w(z) \cdot \mu_{j}^{2}(z) \cdot dz}{\int_{0}^{h} m(z) \cdot \mu_{j}^{2}(z) \cdot dz}\right)$$
(4)

Also note that the tower of height h is divided into a number of zones z in order to apply Eq. 4 where ζ_a is the accumulative aerodynamic damping for all tower zones, ρ_a is the density of air in kg/m^3 , f_T is the frequency of the mode shape in which the structure is excited in Hz, \bar{U} , C_D , w, μ_j and m are the mean wind speed (in m/s), drag coefficient, width (in m), mode shape and mass (in kg) of zone z, respectively. \bar{U} could be obtained using the power law for the appropriate terrain

exposure, C_D is calculated from the solidity ratio of the tower based on ASCE 74 (2010), and μ_j could be acquired from structural dynamics of a SDOF system (Holmes, 1994, 1996a).

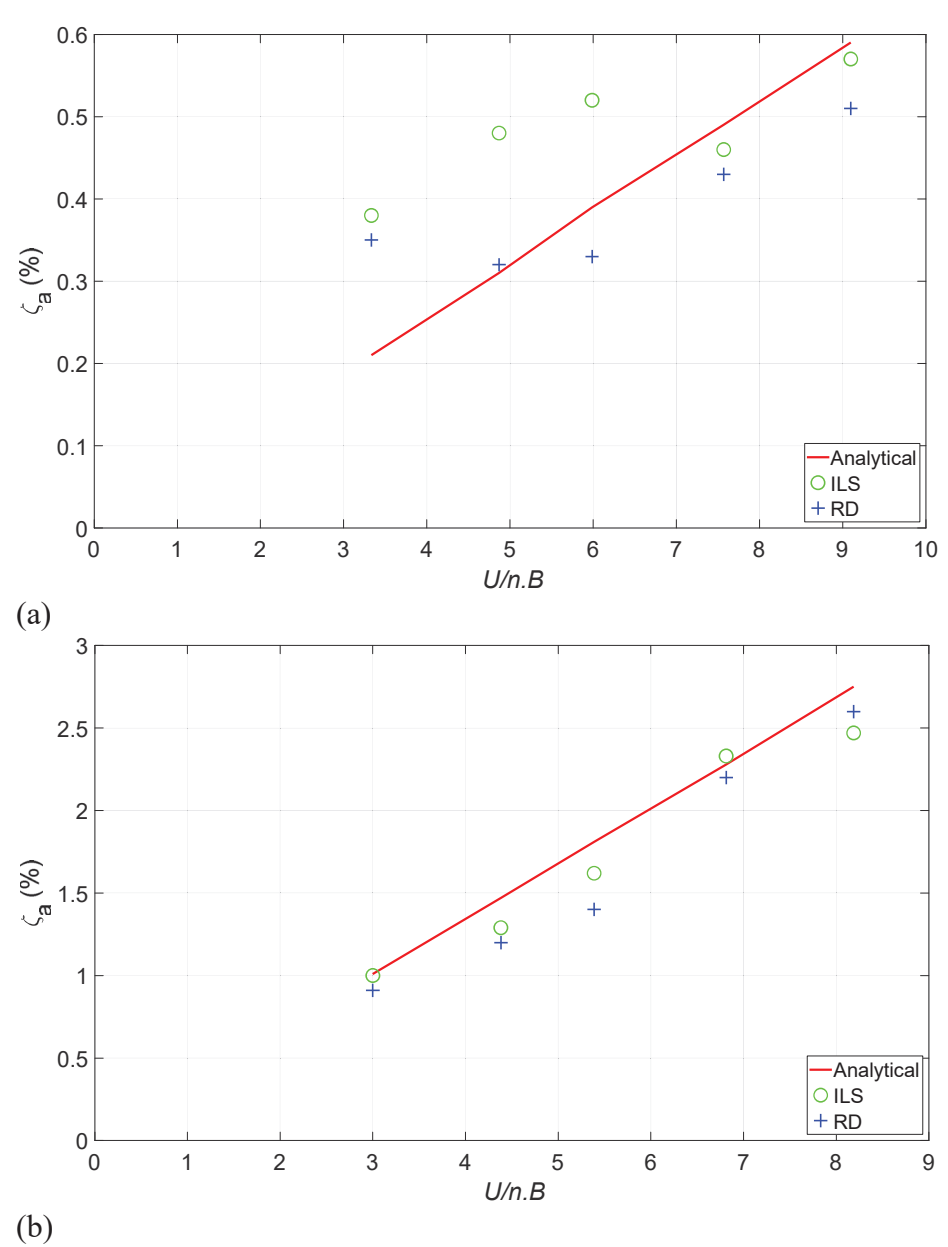


Fig. 9: Along-wind aerodynamic damping values at: (a) 0° wind direction, and (b) 90° wind direction

Fig. 9a and 9b show that the damping values estimated using the ILS and RD techniques agree very well with values computed using the analytical equation proposed by Loredo-Souza and Davenport (2003), especially for the 90° wind direction. At 0° wind direction, there is a discrepancy at lower wind speeds, but the results converge at higher speeds. It is worthwhile men-

tioning that the variance of the damping ratio estimated from measured response data can reach up to 70%. Such a difference is attributed to the number of estimation methods available and the accuracy of the selected technique [(Haviland, 1976); (Davenport, 1983); (Takeuchi et al., 2010)].

The crosswind aerodynamic damping of the lattice tower for 0° and 90° wind directions is presented in Fig. 10. Generally, there is no recommendation on the crosswind aerodynamic damping of lattice structures and standards mostly design for the along-wind direction only. Consequently, the cross wind ζ_a is commonly assumed to be zero, and no analytical method has been developed in order to check the adequacy of such a statement. Furthermore, the Australian standard for design of steel lattice towers AS 3995 (1994) specifically states that the crosswind response of lattice structures can be neglected if the solidity ratio ϕ is less than 0.5 in that direction. When ϕ is greater than 0.5 (such as near the top of lattice towers where diagonal members are very close to each other), structural effects due to a combination of along-wind and crosswind responses must be considered, in accordance with AS/NZS 1170.2 (2011). More research studies are needed to assess the validity of these recommendations together with the inherent assumptions.

Fig. 10 shows that ζ_a changes sign with the increase in the wind speeds. For 0° wind direction, the crosswind aerodynamic damping starts off as negative then rises with increasing wind speeds. For 90° wind direction, ζ_a is positive at low wind speeds and gradually decreases with increasing wind speeds. Note that the solidity ratio ϕ of the lattice tower in this study is about 0.35 for wind along the weak axis and 0.47 for wind along the strong axis. Surprisingly, the values of ζ_a switched signs at a U/(n.B) of about 4.8 for both wind directions. This behavior concerning the crosswind response was previously observed and documented in the literature by

Marukawa et al. (1996) and Huang et al. (2013) in their experimental assessment of the aerodynamic damping of typical tall buildings. This observation was reported for tall buildings having a length to width ratio of 2.5, almost identical to the ratio of the hollow spine rectangular dimensions in this study. This indicates that the presence of the spine may have affected the crosswind aerodynamic damping in the present tests.

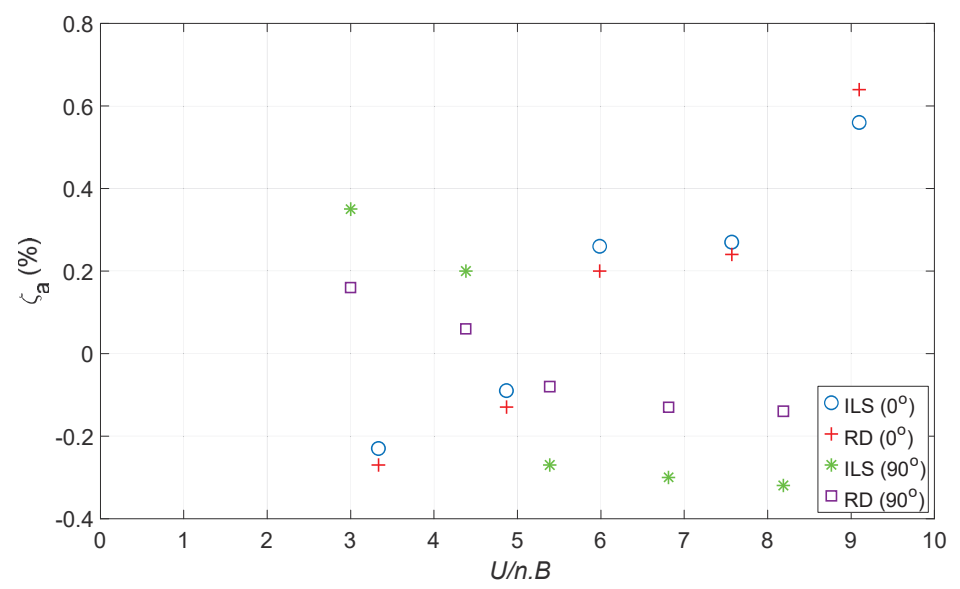


Fig. 10: Crosswind aerodynamic damping for two wind directions (0° and 90°)

3.2 **Buffeting Theory and Comparison between Analytical and Experimental Results**

This section discusses the theoretical buffeting of a flexible slender structure. By conducting a buffeting analysis of the response of the tower in both longitudinal and transverse directions, one can estimate the theoretical root-mean-square (RMS) values of acceleration, base shear, and base moment fluctuations. Consequently, values could be compared with experimentally recorded ones by the 3-axis accelerometers and the 6-DOF load cell. However, in order to perform the buffeting analysis of the lattice tower, some assumptions need to be made:

• The different elements and angles of the lattice tower are small in cross-section so that they do not greatly disturb the flow.

• Using a quasi-steady approach, the fluctuating wind loads can be determined from the aerodynamic force coefficients measured in a steady flow.

- The motions involved in the natural modes of vibration are purely in the along-wind direction. The analysis will be done for two along-wind directions: 0° and 90°, i.e., along both strong and weak axes, respectively.
 - In calculating the RMS accelerations, the lattice tower is treated as a 1-DOF rectangular spine with a fixity at the bottom. The tower assumes all the physical and geometric properties of the spine.
- In calculating the RMS base shears and base moments, equations developed by Loredo-Souza (1996) are adopted and comparisons are made with measured values. Modifications to the equations developed by Loredo-Souza (1996) are then proposed in this study. In its most simplified form, the power spectrum of deflection S_q at the top of the tower is
- 435 given by Eq. 5 [(Davenport, 1962a, 1962b); (Irwin, 1977, 1979, 1996)]:

$$S_q(n) = \frac{(\rho. U. C_{x0}. A)^2}{M_c^2 \omega_0^4} \cdot \left| H\left(\frac{n}{n_0}, \zeta_{tot}\right) \right|^2 \cdot \left| \chi_y(n) \right|^2 \cdot \left| \chi_{2D}(n) \right|^2 \cdot S_u(n)$$
 (5)

In Eq. 5, the density of air ρ is in kg/m³, the wind speed U at tower height h is in m/s, C_{xo} and A are the drag coefficient and frontal effective area in m² of both the spine and the cladding elements, respectively. The generalized mass of the system M_G is in kg and the angular frequency of the system ω_o is in rad/s. Furthermore, n and n_o are the forcing and natural frequencies in Hz, ζ_{tot} is the total damping of the structure (i.e., the structural plus the aerodynamic) (estimated in section 3.2), $H(n/n_o, \zeta_{tot})$ is the mechanical admittance function, $\chi_v(n)$ and $\chi_{2D}(n)$ are the lateral and two-dimensional aerodynamic admittance functions, respectively. Additionally, $S_u(n)$ is the power spectrum of the longitudinal velocity time history. If Eq. 5 is integrated over the range of the forcing frequencies, one can obtain the variance of the deflection fluctuations σ_q^2 from the

power spectrum, and the RMS of the deflection σ_q can then be expressed in terms of background and resonant terms using Eq. 6:

$$\sigma_q = \frac{\rho \cdot U^2 \cdot C_{x0} \cdot A \cdot I_u}{M_G \cdot \omega_0^2} \cdot \sqrt{B + R}$$
(6)

- where I_u is the longitudinal turbulence intensity whereas B and R are the background and reso-
- nant terms. Subsequently, using structural dynamics principles, the RMS of acceleration σ_{acc} may
- be obtained by multiplying Eq. 6 by the square of the angular frequency ω_o , as shown in Eq. 7:

$$\sigma_{acc} = \frac{\rho \cdot U^2 \cdot C_{x0} \cdot A \cdot I_u}{M_G} \cdot \sqrt{B + R} \tag{7}$$

The background and resonant responses (B and R) are defined in Eq. 8 and 9, respectively.

$$B = \int_{0}^{+\infty} |\chi_{y}(n)|^{2} \cdot |\chi_{2D}(n)|^{2} \cdot \frac{S_{u}(n)}{\sigma_{u}^{2}} \cdot dn$$
(8)

$$R = \left| \chi_{y}(n_{o}) \right|^{2} \cdot \left| \chi_{2D}(n_{o}) \right|^{2} \cdot \frac{n_{o} \cdot S_{u}(n_{o})}{\sigma_{u}^{2}} \cdot \frac{\pi}{4 \cdot \zeta_{tot}}$$

$$(9)$$

- with σ_u^2 being the variance of the velocity time history. Note that n_o is the natural frequency of
- 452 the structure in the relevant mode shape. The rest of the parameters of Eq. 8 and 9 are defined in
- 453 Eq. 10 and 11.

$$\left|\chi_{y}(n)\right|^{2} \cdot \left|\chi_{2D}(n)\right|^{2} = \frac{8}{\eta_{b}^{2} \cdot \eta_{d}^{2} \cdot \eta_{L}^{2}} \cdot (\eta_{b} - 1 + e^{-\eta_{b}}) \cdot (\eta_{d} - 1 + e^{-\eta_{d}}) \cdot (\eta_{L} - 1 + e^{-\eta_{l}})$$

$$(10)$$

$$\frac{n_0. S_u(n_0)}{\sigma_u^2} = \frac{4. \frac{n_0. L_u}{U}}{(1 + 70.78(\frac{n_0. L_u}{U})^2)^{5/6}}$$
(11)

In the previous equations, η_b , η_d and η_L are parameters linked to the width, depth and length of the structure and are defined in Eq. 12, 13 and 14, respectively. xL_u , yL_u and zL_u are the integral length scales of longitudinal, lateral, and vertical components of turbulence in m, respec-

tively, whereas d is the depth of the spine in m. Likewise, θ can be taken as 0.75 and b as well as d are the width and length of the rectangular spine in m.

$$\eta_b = 0.95\theta \cdot \frac{b}{{}^{x}L_u} \cdot (1 + 70.78(\frac{n. {}^{x}L_u}{U})^2)^{1/2}$$
(12)

$$\eta_d = 0.475\theta \cdot \frac{d}{{}^{z}L_u} \cdot (1 + 70.78(\frac{2n. {}^{z}L_u}{U})^2)^{1/2}$$
(13)

$$\eta_L = 0.475\theta \cdot \frac{L}{\nu_{L_u}} \cdot (1 + 70.78(\frac{2n. \ ^{y}L_u}{U})^2)^{1/2}$$
(14)

Using Eq. 7, the RMS of acceleration time histories σ_{acc} are calculated for different wind speeds, and values are compared with their experimental counterparts. Fig. 11 presents the results of the buffeting analysis along with the experimental values of the RMS accelerations, recorded by the sensors for two wind directions: 0° and 90° .

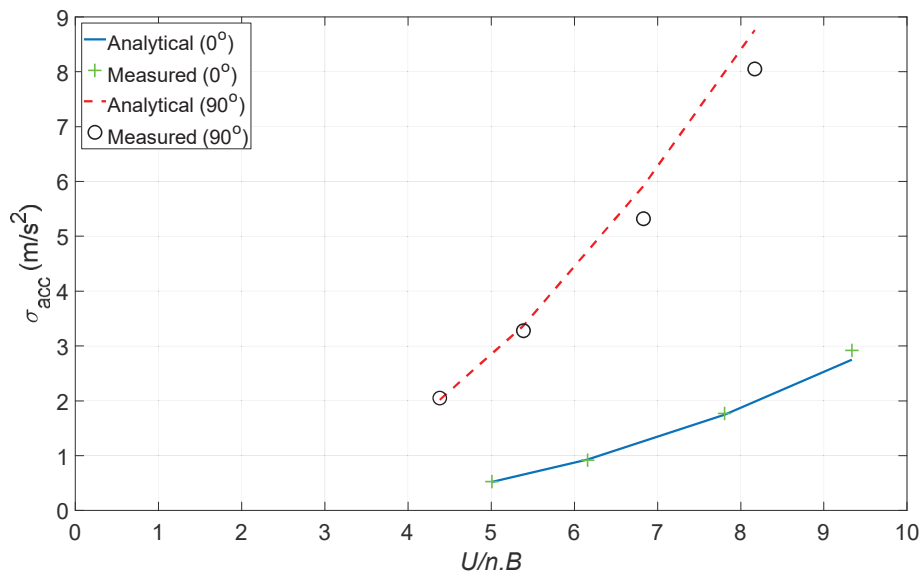


Fig. 11: Comparison of analytical and measured RMS of accelerations for 0° and 90°

It can be observed in Fig. 11 that, at 0° wind direction, the analytical and measured responses show almost complete agreement for all reduced velocity values. At 90° wind direction, Fig. 11 shows good agreement between the measured data and the analytical model at lower speeds. However, some divergences start to appear with increasing wind speeds. This is ex-

plained by the observed crosswind vibrations of the model during the wind testing. This phenomenon reduces the deflection of the model in the along-wind direction (at 90°), thereby reducing the recorded values of σ_{acc} . Since the buffeting theory only addresses along-wind responses, this phenomenon is not accounted for. Nonetheless, the measured and calculated values are very satisfactory for both wind directions.

Similarly, a buffeting analysis was conducted in order to estimate the RMS base shears and base moments at different wind speeds. According to Loredo-Souza (1996) and Loredo-Souza and Davenport (2003), the total fluctuating response (RMS) of forces on a self-supported lattice tower is equal to the square root of the sum of the squares of the background and resonant responses, as shown in Eq. 15. The expressions for the background and resonant responses are given in Eq. 16 and 17, respectively.

$$\sigma_{for} = \sqrt{\sigma_{B,for}^2 + \sigma_{R,for}^2} \tag{15}$$

$$\sigma_{B,for} = \sqrt{(\rho. U_h^2. I_u)^2. I_1}$$
(16)

$$\sigma_{R,for} = \sqrt{\frac{\pi}{4} \cdot \frac{n.S_F(n)}{\zeta_{tot}}} \cdot \frac{\int_0^h m(z) \cdot \mu_j(z) \cdot i(z) \cdot dz}{\int_0^h m(z) \cdot \mu_j^2(z) \cdot dz}$$
(17)

In Eq. 16, U_H is the mean wind speed at tower height h in m/s and I_I is the value of the first double integral, defined in Eq. 18. Similarly, in Eq. 17, $n.S_F(n)$ is the spectrum of the generalized force, given in Eq. 19 and m(z), $\mu_J(z)$, and i(z) are the respective mass per unit height (in kg/m), mode shape and influence line per zone z along the height of the tower.

$$I_{1} = \int_{0}^{h} \int_{0}^{h} C_{D}(z)C_{D}(z')\phi(z)\phi(z') \left(\frac{z}{h}\right)^{\alpha} \left(\frac{z'}{h}\right)^{\alpha} e^{-\left(\frac{\Delta z}{z_{L_{u}}}\right)} i(z)i(z')w(z)w(z')dzdz'$$
(18)

$$n. S_F(n) = (\rho. \overline{U}_h^2. I_u)^2. \frac{n_0. S_u(n_0)}{\sigma_u^2}. |\chi_{2D}(n_0)|^2. I_2$$
(19)

In Eq. 18 and 19, $C_D(z)$, $\phi(z)$, and w(z) are the drag coefficient, solidity ratio and average width (in m) of zone z, α is the wind shear exponent for open-terrain exposure and Δz is the difference in heights between two zones z and z' along the height of the tower (in m). Note that, for influence lines pertaining to base shear calculation, i(z) of each zone is equal to 1 (Loredo-Souza, 1996). I_2 is the value of the second double integral, given in Eq. 20.

$$I_2 = \int_0^h \int_0^h C_D(z)C_D(z')\phi(z)\phi(z') \left(\frac{z}{h}\right)^\alpha \left(\frac{z'}{h}\right)^\alpha e^{\frac{-c|\Delta z|n_o}{U_{0.5h}}} \mu_j(z)\mu_j(z')w(z)w(z')dzdz'$$
(20)

In Eq. 20, c is the exponential decay factor for "narrow band" correlation (usually taken as 7) and $U_{0.5h}$ is the mean wind speed at mid-height of the tower (0.5h) in m/s. As such, the RMS of base shear force fluctuations σ_{for} are calculated using Eq. 15 and the theoretical and measured results are plotted in Fig. 12 for comparison. The values of σ_{for} have been converted to full-scale using the appropriate factor from Table 1 ($\lambda_F = 50^3$). Note that "Analytical" in the legend of Fig. 12 corresponds to the values calculated from Eq. 15 through 20, developed by Loredo-Souza (1996) and Loredo-Souza and Davenport (2003).

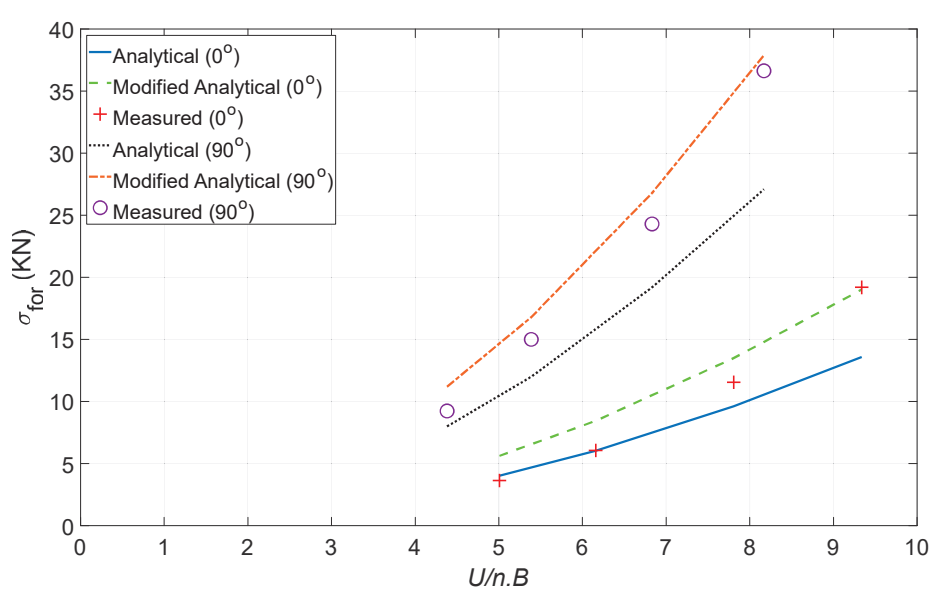


Fig. 12: Comparison of analytical and measured RMS of forces for 0° and 90°

As shown in Fig. 12, the "Analytical" values of σ_{for} tend to underestimate the measured response of the aeroelastic model at almost all tested wind speeds. This observation is evident, especially at 90° wind direction, where the divergence becomes wider with increasing wind speeds. At 0° wind direction, the analytical results show good agreement at low values of U/(n.B). The discrepancies between the measured and calculated σ_{for} can be attributed to the turbulence intensity I_u factor at tower height h, shown in Eq. 16 and 19. Typically, the turbulence intensity is much higher near ground surface and reduces significantly with increasing height. As such, this change in intensity should be accounted for in the equations, in order to get a more realistic estimate of the response of the lattice tower. This would translate into higher calculated values, especially in the lower zones of the tower, potentially resulting in better agreement with the measured response using the 6-DOF load cell. Based on the two cobra probe measurements collected in the experiments of the current study and with the help of ESDU item 85020 (2001) for full-scale turbulence intensity approximation, the authors propose Eq. 21 for use in estimating I_u at any height z:

$$I_u(z) = I_u(h) \cdot \left(\frac{z}{h}\right)^{\gamma} \tag{21}$$

Similarly to the power law used in the wind speed estimation at any height z, Eq. 21 can be used for the estimation of I_u . In the present tests, the exponent γ in Eq. 21 was found to be approximately -0.15. Consequently, the terms $(z/h)^{-0.15}$ and $(z'/h)^{-0.15}$ are added to the double integral values I_1 and I_2 in Eq. 18 and 20 and the buffeting analysis was repeated. The resulting calculated responses are plotted in Fig. 12 and are denoted as "Modified Analytical".

As can be observed in Fig. 12, the agreement with the experimental values at high speeds is much improved compared with the original equations developed by Loredo-Souza (1996). Therefore, it is highly recommended that Eq. 18 and 20 be rewritten as Eq. 22 and 23:

$$I_{1} = \int_{0}^{h} \int_{0}^{h} C_{D}(z)C_{D}(z')\phi(z)\phi(z')\left(\frac{z}{h}\right)^{\alpha+\gamma} \left(\frac{z'}{h}\right)^{\alpha+\gamma} e^{-\left(\frac{\Delta z}{z_{L_{u}}}\right)} i(z)i(z')w(z)w(z')dzdz'$$
(22)

$$I_{2} = \int_{0}^{h} \int_{0}^{h} C_{D}(z)C_{D}(z')\phi(z)\phi(z')\left(\frac{z}{h}\right)^{\alpha+\gamma} \left(\frac{z'}{h}\right)^{\alpha+\gamma} e^{\frac{-c|\Delta z|n_{o}}{U_{0.5h}}}\mu_{j}(z)\mu_{j}(z')w(z)w(z')dzdz'$$

$$(23)$$

Lastly, from the previous equations, one can obtain the theoretical RMS base moment fluctuations from that of the base shear by incorporating the height of the tower and using the appropriate values for the influence lines i(z). In Eq. 16 and 19, the term $(\rho.U_h.I_u)^2$ becomes $(\rho.U_h.I_u.h)^2$. This multiplication of the force by the distance to the base of the tower will yield the overturning moment. Note that, for influence lines pertaining to base moment calculation, i(z) is equal to the height of the zone z divided by the total height of the tower h(z/h). Fig. 13 shows a comparison between measured and calculated values of RMS base moments. Once again, the full-scale values were utilized by multiplying with the appropriate factors from Table 1 ($\lambda_M = 50^4$).

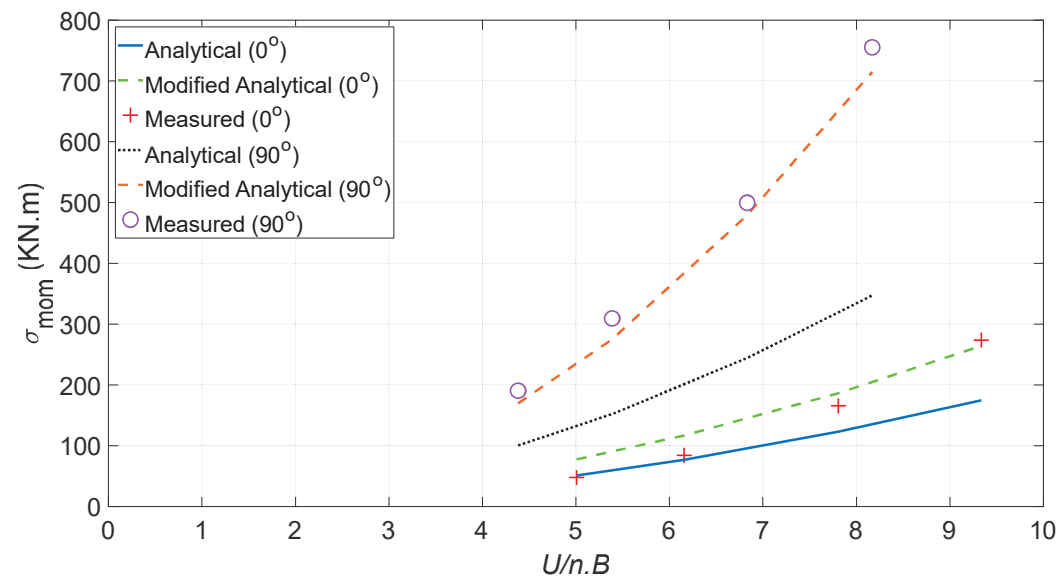


Fig. 13: Comparison of analytical and measured RMS moments for 0° and 90°

As shown in Fig. 13, there is good agreement for both wind directions and the inclusion of the change in turbulence intensity along the height of the structure was very beneficial. In

summary, the agreement is very satisfactory for the along-wind RMS accelerations, base shears, and base moments for both wind directions 0 and 90 degrees.

3.3 **Drag and Moment Coefficients**

This subsection discusses the calculation of the drag and moment coefficients obtained from the measured strain data and subsequent comparison with values proposed by standards from different countries around the world. Theoretically, according to ASCE 7 (2016), the drag coefficient C_D and the moment coefficient C_M are defined in Eq. 24 and 25, respectively.

$$C_D = \frac{F_D}{\frac{1}{2}\rho. U^2. A} \tag{24}$$

$$C_M = \frac{M_o}{\frac{1}{2}\rho. U^2. A. h} \tag{25}$$

In Eq. 24 and 25, F_D is the mean drag force in N, M_o is the mean overturning moment in N.m (measured at the base), A is the net area in m^2 , and h is the height of the structure in m. The rest of the parameters were defined earlier.

Experimentally, the drag coefficients can be estimated based on the data collected from the strain gauges installed on different parts of the spine. By definition, the maximum bending stress at any point in a structure can be expressed using Eq. 26.

$$\sigma = \frac{M.c}{I} \tag{26}$$

In Eq. 26, *M* is the measured bending moment at the point of location in N.m, *c* is the distance from the extreme most fiber to the centroid of the section in m, and *I* is the moment of inertia of the section about the axis of bending in m⁴. Using Hook's law and assuming that the spine section of the tower remains elastic, Eq. 27 (Azzi et al., 2020b) can be used to obtain the strain at any point.

$$\varepsilon = \frac{M.b}{2E.I} \tag{27}$$

In Eq. 27, ε is the strain in the direction of the loading, E is the modulus of elasticity of the spine in N/m² and b is the distance to the centroid in m.

Fig. 14 shows a sketch of the forces acting on the spine. It is important to note that, during the design stage of the model, and more specifically for the cladding elements, the tower geometry was divided into seven zones. Each zone had its own drag coefficient, based on its solidity ratio. For the sake of this study, the drag coefficients of the entire tower are assessed with respect to both wind speeds and directions.

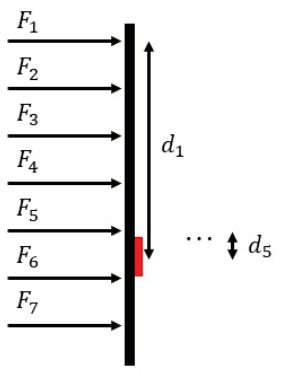


Fig. 14: Forces applied on the spine (strain gauge shown in red)

From Fig. 14, the measured bending moment M at the location of the strain gauge mounted on the spine can be expressed using Eq. 28 (Azzi et al., 2020b).

$$M = \sum_{i=1}^{5} F_{Di}. d_i = \sum_{i=1}^{5} \frac{1}{2} \rho. A_i. C_D. U_i^2. d_i = \frac{1}{2} \rho. C_D. \sum_{i=1}^{5} A_i. U_i^2. d_i$$
 (28)

In Eq. 28, i represents the zone number above the strain gauge, U_i is the wind speed at the height of the zone in m/s, A_i is the area of the elements in the plane perpendicular to the wind direction in zone i in m² and d_i is the distance from the strain gauge to the point of application of the force on zone i, in m. Note that a total of five zones are above the strain gauge portrayed in red in Fig. 14. Combining Eq. 27 and 28, the drag coefficient can be experimentally obtained using Eq. 29.

$$C_D = \frac{4 \cdot \epsilon \cdot E \cdot I}{b \cdot \rho \cdot \sum_{i=1}^5 A_i \cdot U_i^2 \cdot d_i}$$
 (29)

Similarly, and for squared trussed towers such as the case of lattice towers, ASCE 7 (2016), ASCE 74 (2010), and ANSI/TIA-222 (2005) suggest Eq. 30 for the calculation of the force coefficients (or drag coefficients per zone). Eq. 30 presents C_D as a function of the solidity ratio ϕ , which is defined as the ratio of the solid (or net) area to the gross area of the tower zone, in the direction of the loading. Additionally, the BS EN (2006) suggests Eq. 31 for the calculation of the drag forces on the tower. Note that the previous standards suggest such equations for any tower zone, regardless of its shape.

$$C_D = 4\phi^2 - 5.9\phi + 4 \tag{30}$$

$$C_D = 3.96\phi^2 - 5.94\phi + 3.96 \tag{31}$$

Fig. 15a shows a comparison between the mean drag coefficients obtained using strain gauge experimental data and those specified by the standards. Note that each cross mark on Fig. 15a and 15b represents one solidity ratio obtained from one wind direction acting on the lattice tower (total of seven marks for seven wind directions tested). Also note that the mean drag coefficient values were obtained from the strain gauges whereas the mean moment coefficient values were obtained from the load cell installed at the base of the tower. Examining Fig. 15a, it can be seen that the experimental values of C_D obtained are well in agreement with values obtained using Eq. 30 and 31 of the standards. This trend is seen for all values except for a solidity ratio ϕ of 0.47, i.e., at a wind direction of 0°, where the drag coefficient C_D obtained from the experiment is almost half the value suggested by the standards. Nevertheless, for the rest of the wind directions, the C_D values are well in range of the theoretically suggested ones.

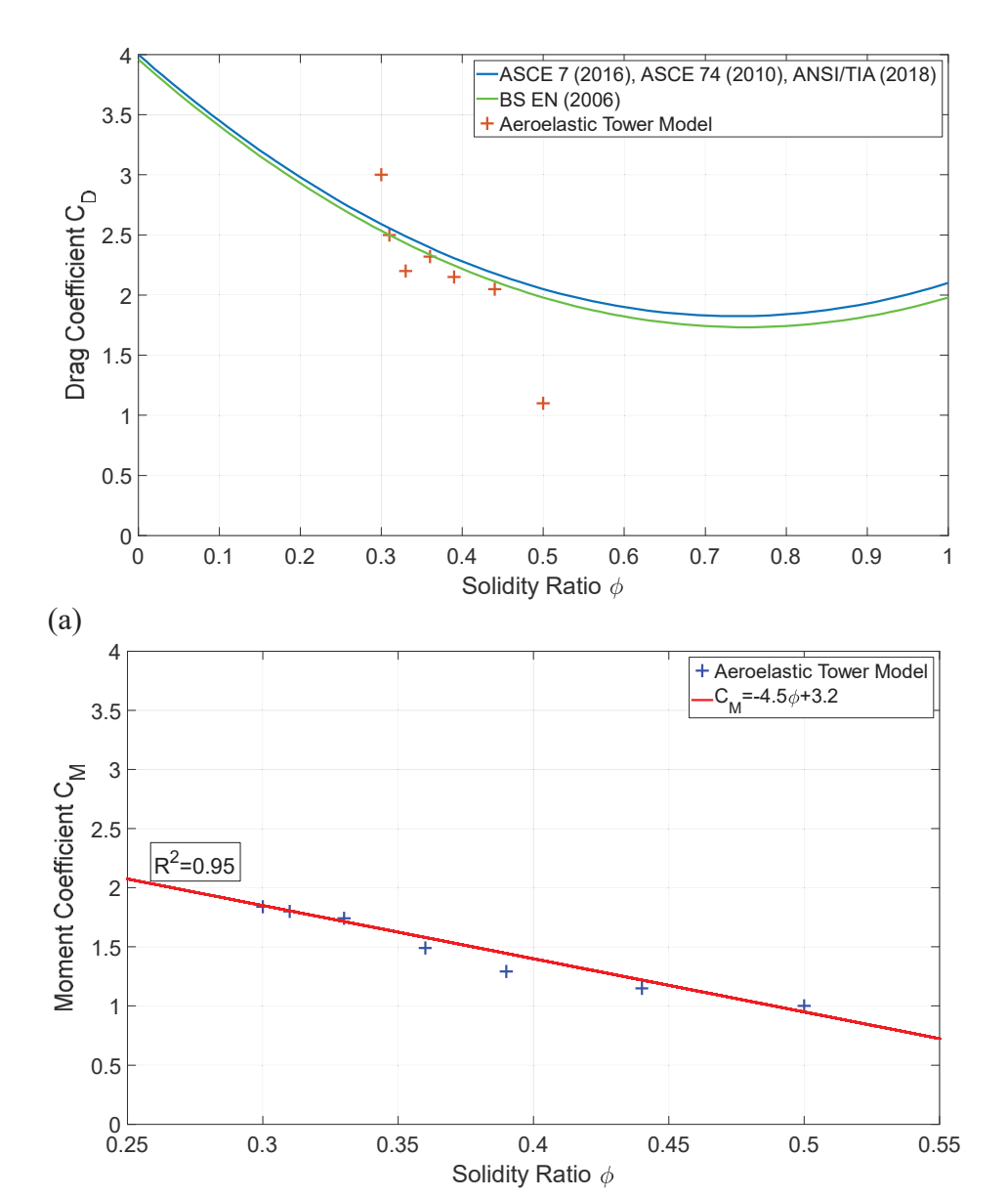


Fig. 15: Values of: (a) drag coefficient C_D , and (b) moment coefficient C_M

Since lattice towers are truss structures, design standards treat them as perfect trusses with frictionless hinged connections in between angles and members. Therefore, to the authors' best knowledge, no previous studies addressed the moment coefficients in the design of lattice structures.

However, the actual type of connection between such truss members might differ. Previous researchers have shown that typical truss connections could be single bolted, multiple bolted,

welded using a gusset plate, or using a combination of welds and bolts. Such connection types often have a degree of rigidity, therefore introducing potential bending moments and possible twist [(da Silva et al., 2005); (Zhangqi et al., 2014); (Axisa et al., 2017)].

Fig. 15b shows that the values of C_M tend to linearly decrease with the increase of the solidity ratio. Therefore, a first-degree polynomial equation is proposed with a R-squared value of 0.95, linking the moment coefficient to the solidity ratio. The latter is presented in Eq. 32 and plotted in Fig. 15b:

$$C_M = -4.5\phi + 3.2 \tag{32}$$

It is worthwhile noting that, typically, the solidity ratio of lattice towers ranges between 0.2 and 0.6. For the tower tested at the WOW, the solidity ratio ranged between 0.3 and 0.5. Therefore, Eq. 32 might be only valid for the range of solidity ratios tested in this project. Thus, more research and testing are required in order to better understand the behavior of truss joints and to provide a better moment coefficient equation for design purposes. This would potentially reduce the failure of connection members in lattice structures, which are commonly used not just in civil engineering as transmission towers, but also in telecommunication as radio towers and mechanical engineering as wind turbine supports, among others.

3.4 Dynamic Amplification and Gust Effect Factors

This last subsection discusses the Dynamic Amplification Factor (DAF) relevant to lattice structures. This factor defines the ratio between the maximum peak and the quasi-static responses. According to Elawady et al. (2017) and Azzi et al. (2020c), the DAF is given in Eq. 33:

$$DAF = \frac{Maximum\ Peak\ Response}{Maximum\ Quasi-static\ Response}$$
(33)

In Eq. 33, the quasi-static response is defined as the summation of the mean and the background responses. Note that, on one hand, the resonant response is associated with resonant amplifica-

tion due to components (forces or moments) with frequencies close or equal to the fundamental natural frequency of the structure in the desired mode. On the other hand, the background response involves no resonant amplification [(Simiu and Yeo, 2019); (Azzi et al., 2020c)].

However, it should be noted that the entire procedure revolves around the concept that the fluctuating response is excited by the fluctuating wind field. Detailed steps for the calculation of the DAF can be found in Elawady et al. (2017) and Azzi et al. (2020c). Values of DAF are generated for the forces and moments acting on the lattice tower as well as for axial forces in the cross-arms. Fig. 16a shows a sample of the signal decomposition process that was applied to all recorded time histories. This figure shows the decomposition of base moment M_y . Fig. 16b shows a zoomed in plot of the resonance detected in Fig. 16a. More information and detailed description on the DAF method is available in Elawady et al. (2017).

Some response measurements have shown a high contribution of the resonant component while others did not. As can be seen in Fig. 16a, the slope of the cumulative PSD of the base moment about the weak axis (drawn in green) shows a sudden steep behavior when the resonance is detected (blue circles) around the natural frequency of the structure (mode shape 1, around 16 Hz, Table 2). This means that the resonant component significantly contributes to the structural response at that particular frequency. This can be seen in Fig. 16b where the resonance is detected between about 13 Hz and 16.5 Hz (blue circles). The DAF values for the rest of the responses (F_x , F_y , M_x , M_y , P_{arm}) are plotted in Fig. 17.

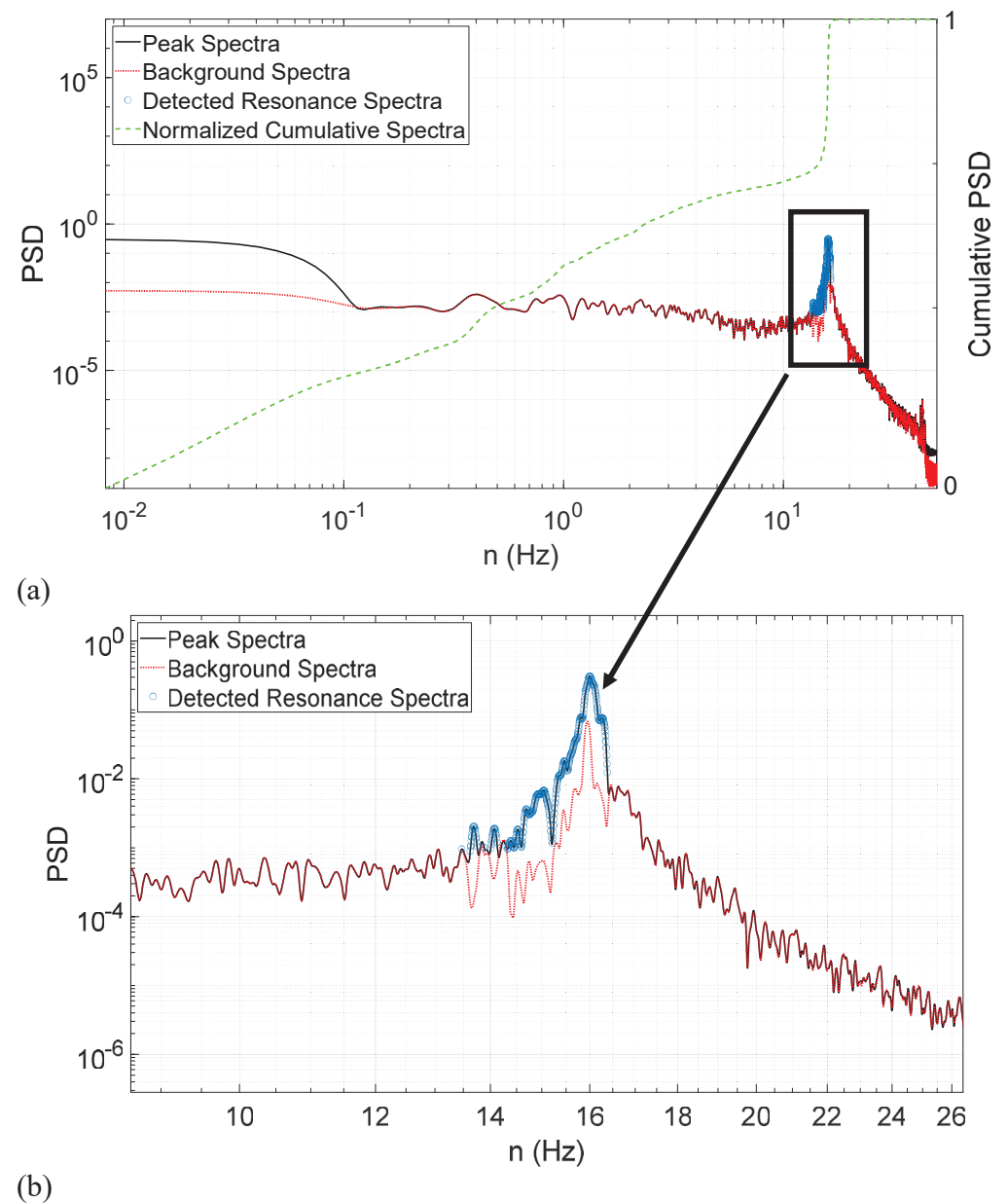


Fig. 16: Decomposition of the base moment M_y time history (about weak axis): (a) initial plot, and (b) resonance detection (zoomed in plot of Fig. 16a)

The DAF values of all measured responses are shown in Fig. 17 to range between 1.01 and 1.18. It can be seen that DAF values of the base shears F_x and F_y decrease with increasing wind speeds. This is due to the increase in the aerodynamic damping which was reported in the previous sections. This phenomenon slightly suppresses the resonant component, thereby reducing its contribution to the total response of the entire structure. The DAF values of the base moments M_x and M_y are shown to increase with increasing wind speeds. The previously mentioned

excessive vibrations observed at particularly higher wind speeds, especially in the crosswind direction, might have played a role in altering the behavior of the DAF values of the moments, thereby overshadowing the effect of the increase in the aerodynamic damping.

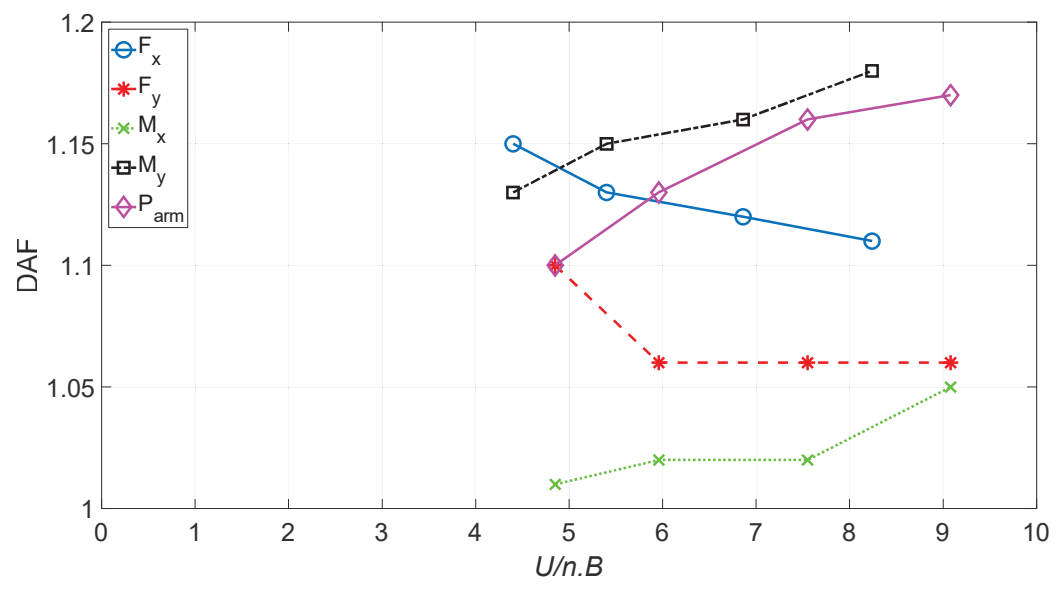


Fig. 17: DAF values for base shears, base moments, and cross-arm axial force

Finally, the DAF values of the cross-arm force P_{arm} are also shown to increase with increasing wind speeds. This was also noted by Elawady et al. (2017) for the case of a single lattice structure. This is possibly due to the relatively higher flexibility of the cross-arm system compared to other zones in the tower structure. Since such a tower configuration is typically used as part of a tower-insulator-conductor transmission line system, the absence of the conductors (which are typically attached to the cross-arms and provide lateral bracing at the insulator-conductor connection points) might have led to excessive vibrations and bending in the cross-arm itself. Subsequently, an increase in the resonant contribution to the total response of the cross-arms is to be expected with increasing wind speeds.

On another note, in any wind engineering analysis, the fluctuating component is coming from the background and resonant responses, as shown in Eq. 34:

$$\widehat{D} = \overline{D} + D_B' + D_R' \tag{34}$$

In Eq. 34, \hat{D} , \bar{D} , D'_B , D'_R are the peak, mean, background and resonant components of any response D. Since the DAF values are defined as the ratio of the peak (\hat{D}) over the summation of the mean and background components $(\bar{D} + D'_B)$ (Eq. 33) and the Gust Response Factors G, developed by Davenport (1979) are defined as the ratio of the peak (\hat{D}) over the mean (\bar{D}) , then Eq. 35 could be used to link the DAF to G.

$$G = DAF(1 + \frac{D_B'}{\overline{D}}) \tag{35}$$

Note that, in order to compare with design standards such as ASCE 7 (2016) and ASCE 74 (2010), *G* needs to be adjusted by the Gust Velocity Factor as shown in Eq. 36. As such, *G* becomes the Gust Effect Factor *G'*. As noted by Solari and Kareem (1998), *G'* in codes is used for a threefold purpose: (i) to reduce the wind load due to the non-contemporaneous wind action through the aerodynamic admittance function, (ii) to account for the resonant amplification of structural responses due to turbulence, and (iii) to facilitate determination of design peak effects using code design wind speed (usually 3-sec gust) in conjunction with coefficients that were obtained in wind tunnels using wind speeds with different averaging times. Note that the reference wind speed in the denominator of Eq. 36 is for a 14-min period since our tests are representative of a 14-min event in full-scale (section 2.3).

$$G' = \frac{G}{\left(\frac{U_{3se}^2}{U_{14min}^2}\right)} \tag{36}$$

In comparison with standards, ASCE 74 (2010) has established a tower and conductor gust response factors G_T and G_C , respectively, in order to account for any dynamic effects on lattice towers used as transmission lines as well as electrical conductors. By definition, the gust response factors G_T and G_C are the ratios of the peak load effect on the structure or conductors to

the mean load effect corresponding to the design wind speed (typically, the 3-sec gust) (ASCE 74, 2010).

For this study, the current interest rests with the tower gust response factor G_T . ASCE 74 (2010) uses Eq. 37 to obtain G_T and the 3-sec gust wind speed is used in the design of transmission towers by utility companies. Also note that G_T is based on the original gust response factors, developed by Davenport (1979).

$$G_T = \frac{1 + 2.7E \cdot \sqrt{B_t}}{K_t^2} \tag{37}$$

In Eq. 37, K_u refers to the ratio of the 3-sec gust wind speed to the 10-min average wind speed (usually taken as 1.43) while parameters E and B_t are given in Eq. 38 and 39.

$$E = 4.9.\sqrt{\kappa}.\left(\frac{33}{z_h}\right)^{1/\alpha_{ter}} \tag{38}$$

$$B_t = \frac{1}{1 + \frac{0.56z_h}{L_s}} \tag{39}$$

The rest of the parameters of Eq. 38 and 39 are given in ASCE 74 (2010) section 2.1.5.1 for different exposure categories. Using the values proposed in ASCE 74 (2010) for open terrain exposure, the value of G_T for the transmission tower tested in this project comes out to about 0.88. The G_T values are compared to G', computed for all measured responses using Eq. 35 and 36, and the results are presented in Fig. 18. As can be seen in Fig. 18, the obtained G' for all measured responses are below the G_T values proposed in ASCE 74 (2010) for all U/(n.B). For the case of M_Y and P_{arm} , there is a small exceedance at values of U/(n.B) higher than 8. But the exceedance is less than 5%. This shows that values of G_T proposed in the standard are adequate. However, this statement might be true only for this tower configuration and shape. In addition, the use of such tower in a transmission line system (i.e., with the addition of conductors on either

side of the tower) might change the obtained results due to the increase in the complexity of the system and the added drag on the conductors. Therefore, there is a need to evaluate the above for transmission line systems as well.

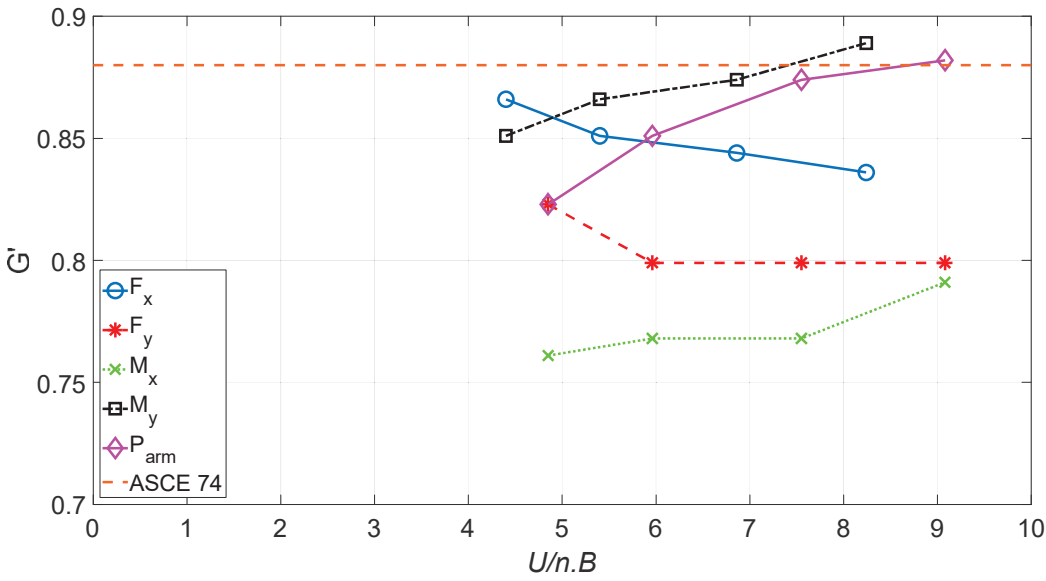


Fig. 18: Corresponding G' values for base shears, base moments, cross-arm axial force and comparison with G_T

4 Conclusion

Estimation of wind effects on a single self-supported lattice tower using aeroelastic testing at the NHERI WOW EF has been described. The lattice tower considered is a typical structure that is used as part of a tower-insulator-conductor system for electrical transmission. The model was first designed and validated using FEM analysis, then constructed using a spine structure and non-structural cladding elements. The spine structure represented the elastic flexural and torsional properties of the tower whereas the cladding elements formed its aerodynamic shape. The model length and velocity scales selected were 1:50 and 1:7.07, respectively.

The major findings from this research are summarized below:

- The estimated along-wind aerodynamic damping coefficients using the ILS and RD techniques were in very good agreement with their analytical counterparts for both main directions (normal and parallel to transmission span).
- The crosswind aerodynamic damping might be important for lattice tower design.
- The buffeting analysis results showed good agreement with the measured alongwind RMS responses of the tower. It was found that incorporating the variation of turbulence intensity along the height yields some improvements over the original analytical approach.
- The drag coefficients were in good agreement with those given in many standards adopted around the world.
- The implementation of moment coefficients for the wind design of lattice structures could prove important.
- Calculated DAF values showed that the resonant response of the tower is in the order of 1% to 18% for all measurements and the calculated gust effect factor G' is well in agreement with the tower response factor G_T suggested in ASCE 74 (2010).

Finally, this paper focused on one type of lattice structures only. Other lattice structure configurations with varying solidity ratios should also be investigated for dynamic behavior under high winds. It would be worthwhile looking at the effects of topography (such as regions will hills and escarpments) change on the behavior of the tested structure.

Acknowledgments

708

709

710

711

712

713

714

715

716

717

718

719

720

721

722

723

724

725

726

727

728

729

730

The authors greatly acknowledge the help offered by Mr. Walter Conklin and Mr. Roy Liu-Marques in conducting the experiments at the NSF NHERI WOW EF (NSF Award No.

- 731 1520853). This research is supported by an NSF award (NSF Award No. 1635569). Funding
- from the Florida International University Graduate School (FIU UGS) Dissertation Year Fellow-
- ship (DYF) is greatly appreciated. The opinions, findings, and conclusions expressed in this pub-
- 734 lication are those of the authors and not necessarily those of the funding agencies.

735 References

- Aboshosha, H., Elawady, A., El Ansary, A., and El Damatty, A. (2016). "Review on dynamic
- and quasi-static buffeting response of transmission lines under synoptic and non-synoptic
- 738 winds." Engineering Structures, 112, 23-46.
- 739 American National Standards Institute (ANSI) / Telecommunications Industry Association
- 740 (TIA), ANSI/TIA-222-G (2005). "Structural Standard for Antenna Supporting Structures and
- Antennas." Standards and Technology Department, Arlington, VA, U.S.A.
- American Society of Civil Engineers (ASCE) 74 (2010). "Guidelines for electrical transmission
- line structural loading." ASCE manuals and reports on engineering practice, No. 74, New
- 744 York, NY, USA.
- American Society of Civil Engineers (ASCE) 7 (2016). "Minimum Design Loads and Associated
- 746 Criteria for Buildings and Other Structures." ASCE/SEI 7-16, Reston, VA.
- 747 Australian/New Zealand Standard (AS/NZS) 1170.2 (2011). "Structural design actions Part 2:
- 748 wind actions." SAI Global Limited, Standards Australia Limited, GPO Box 476, Sydney,
- NSW 2001, Standards New Zealand, PO Box 1473, Wellington 6140.
- Australian Standard (AS) 3995 (1994). "Design of steel lattice towers and masts." Standards As-
- sociation of Australia, The Crescent, Homebush, NSW 2140.
- Axisa, R., Muscat, M., Sant, T., and Farrugia, R. N. (2017). "Structural assessment of a lattice
- tower for a small, multi-bladed wind turbine." International Journal of Energy and Environ-
- mental Engineering, 8, pp. 343-358.
- 755 Azzi, Z. (2016). "Behavior of Un-reinforced Concrete Masonry Infill Walls under Lateral Earth-
- quake Loads." Lebanese American University (LAU) Repository, School of Engineering
- 757 (SOE) Theses and Dissertations.
- Azzi, Z., Habte, F., Elawady, A., Chowdhury, A. G., and Moravej, M. (2020a). "Aerodynamic
- 759 Mitigation of Wind Uplift on Low-Rise Building Roof Using Large-Scale Testing." Frontiers
- in Built Environment, Wind Engineering and Science, 5:149.
- 761 Azzi, Z., Elawady, A., and Chowdhury, A. G. (2020b). "Large-Scale Aeroelastic Testing to In-
- vestigate the Resiliency of Transmission Infrastructure to Hurricane Storms." Proceedings of
- the 11th International Conference on Structural Dynamics (EURODYN 2020), Athens,
- 764 Greece, November 23-26, pp. 1944-1957.

- Azzi, Z., Matus, M., Elawady, A., Zisis, I., Irwin, P., and Chowdhury, A. G. (2020c). "Aeroelastic Testing of Span-Wire Traffic Signal Systems." Frontiers in Built Environment, Wind En-
- gineering and Science, 6:111.
- 768 Azzi, Z., Habte, F., Vutukuru, K. S., Chowdhury, A. G., and Moravej, M. (2020d). "Effects of
- roof geometric details on aerodynamic performance of standing seam metal roofs." Engineer-
- 770 ing Structures, 225, 111303.
- Badruddin Ahmad, M., Pande, P. K., and Krishna, P. (1984). "Self-Supporting Towers under Wind Loads". Journal of Structural Engineering, 110(2): 370-384.
- Bartoli, G., Cluni, F., Gusella, V. and Procino, L. (2006). "Dynamics of cable under wind action:
- Wind tunnel experimental analysis." Journal of Wind Engineering and Industrial Aerody-
- 775 namics, 94, 259-273.
- Bayar, D. C. (1986). "Drag Coefficients of Latticed Towers." Journal of Structural Engineering, 112(2): 417-430.
- Boudreaux, T. P. (1962). "Hurricane Carla vs. Transmission Lines." Civil Engineering and Construction Review, April, pp. 70-72.
- 780 British Standard (BS) 50341 (2001). "Overhead electrical lines exceeding AC 45 kV: Part 1 General requirements Common specifications." London, UK.
- British Standard (BS EN) (2006). "Eurocode 3 Design of steel structures Part 3-1: Towers,
 masts and chimneys." The British Standards Institution, London, United Kingdom.
- Carril Jr., C. F., Isyumov, N., and Brasil, R. M. L. R. F. (2003). "Experimental study of the wind forces on rectangular latticed communication towers with antennas." Journal of Wind Engineering and Industrial Aerodynamics, 91, 1007-1022.
- 787 Chabart, O. and Lilien, J. L. (1998). "Galloping of electrical lines in wind tunnel facilities."
 788 Journal of Wind Engineering and Industrial Aerodynamics, 74-76, 967-976.
- Chen, Y., Pan, L., Pan, F., and Guo, Y. (2014). "Dynamical response of transmission line towers subjected to thunderstorm downbursts based on experimental study." 2014 World Congress
- on Advances in Civil, Environmental and Materials Research (ACEM14), Busan, Korea,
- 792 August 24-28.
- 793 Choi, E. C. C., and Hidayat, F. A. (2002). "Dynamic response of structures to thunderstorm winds." Progress in Structural Engineering and Materials, Wind Response of Structures,
- 795 4:408-416.
- Chopra, A. (2017). "Dynamics of Structures: Theory and Applications to Earthquake Engineering." Prentice Hall/Pearson, 5th Edition.
- Chowdhury, A. G., and Sarkar, P. P. (2003). "A new technique for identification of eighteen flutter derivatives using a three-degree-of-freedom section model." Engineering Structures, 25, 1763-1772.
- Chowdhury, A. G., and Sarkar, P. P. (2004). "Identification of eighteen flutter derivatives of an airfoil and a bridge deck." Wind and Structures, Vol. 7, No. 3, 187-202.

- 803 Chowdhury, A. G., Zisis, I., Irwin, P., Bitsuamlak, G., Pinelli, J.-P., Hajra, B., and Moravej, M.
- 804 (2017). "Large-Scale Experimentation Using the 12-Fan Wall of Wind to Assess and Miti-
- gate Hurricane Wind and Rain Impacts on Buildings and Infrastructure Systems." Journal of
- 806 Structural Engineering, 143(7): 04017053.
- da Silva, J. G. S., Vellasco, P. D. S., de Andrade, S. A., and de Oliveira, M. I. R. (2005). "Struc-
- tural assessment of current steel design models of transmission and telecommunication tow-
- ers." Journal of Constructional Steel Research, 61, 8, pp. 1108-1134.
- Davenport, A. G. (1962a). "The response of Slender Line-Like Structures to a Gusty Wind."
- Proceedings of the Institution of Civil Engineers, 23, 3, 389-408.
- Davenport, A. G. (1962b). "Buffeting of a Suspension Bridge by Storm Winds." Journal of the
- 813 Structural Division (ASCE), 88, 3, 233-270.
- Davenport, A. G. (1979). "Gust response factors for transmission line loading." Proceedings of
- the Fifth International Conference on Wind Engineering (5ICWE), U. E. Cermack, ed., New
- 816 York, 2, 899-909.
- Davenport, A. G. (1983). "The relationship of reliability to wind loading." Journal of Wind En-
- gineering and Industrial Aerodynamics, 13, 3-27.
- Davenport, A. G. (1988). "The response of tension structures to turbulent wind: the role of aero-
- dynamic damping." Proceedings of the First International Oleg Kerensky Memorial Confer-
- ence on Tension Structures, London, England, June 20-22.
- Dempsey, D., and White B. H. (1996). "Winds Wreak Havoc on Lines." Transmission & Distri-
- bution World, June; 48, 6; ProQuest pg. 32.
- 824 Elawady, A., and El Damatty, A. (2016a). "Longitudinal Force on Transmission Towers Due to
- Non-Symmetric Downburst Conductor Loads." Engineering Structures, 127, 206-226.
- 826 Elawady, A., Aboshosha, A., El Damatty, A., and Bitsuamlak, G. (2016b). "Wind Tunnel Test-
- ing of a Multiple Span Aeroelastic Transmission Line Subjected to Downburst Wind." Resil-
- ient Infrastructure, London.
- 829 Elawady, A., Aboshosha, H., El Damatty, A., Bitsuamlak, G., and Hangan, H. (2017). "Aero-
- elastic testing of multi-spanned transmission line subjected to downbursts." Journal of Wind
- Engineering and Industrial Aerodynamics, 169, 194-216.
- 832 Elawady, A., Aboshosha, H., and El Damatty, A. (2018). "Aero-elastic response of transmission
- line system subjected to downburst wind: Validation of numerical model using experimental
- data." Winds and Structures, 27, 2, 71-88.
- 835 ESDU (2001). "Characteristics of the Atmospheric Boundary Layer, Part II: Single Point Data
- for Strong Winds (Neutral Atmosphere)." London: Engineering Sciences Data Unit, Item
- 837 85020.
- Federal Emergency Management Agency (FEMA) (2020) "Hurricane Michael in Florida: Build-
- ing Performance Observations, Recommendations, and Technical Guidance." Mitigation As-
- sessment Team Report, FEMA P-2077.

- Feng, C., Chowdhury, A. G., Elawady, A., Chen, D., Azzi, Z., and Vutukuru, K. S. (2020). "Ex-
- perimental Assessment of Wind Loads on Roof-to-Wall Connections for Residential Build-
- ings." Frontiers in Built Environment, Wind Engineering and Science, 6:10.
- Hamada, A. (2014). "Numerical and Experimental Studies of Transmission Lines Subjected to
- Tornadoes." University of Western Ontario, Electronic Thesis and Dissertation Repository,
- 846 Paper 2479.
- Hamada, A., King, J. P. C., El Damatty, A., Bitsuamlak, G., and Hamada, M. (2017). "The re-
- sponse of a guyed transmission line system to boundary layer wind." Engineering Structures,
- 849 139, 135-152.
- Haviland, R. (1976). "A study of the uncertainties in the fundamental translational periods and
- damping values for real buildings." Evaluation of Seismic Safety of Buildings, Research Re-
- port 5, National Science Foundation (NSF).
- Hiramatsu, K., and Akagi, H. (1988). "The Response of Latticed Steel Towers due to the Action
- of Wind." Journal of Wind Engineering and Industrial Aerodynamics, 30, pp. 7-16.
- Holmes, J. D. (1994). "Along-wind response of lattice towers: part I derivation of expressions
- for gust response factors." Engineering Structures, 16, 4, 287-292.
- 857 Holmes, J. D. (1996a). "Along-wind response of lattice towers: II Aerodynamic damping and
- deflections." Engineering Structures, 18:483-488.
- 859 Holmes, J. D. (1996b). "Along-wind response of lattice towers: III Effective load distribu-
- tions." Engineering Structures, 18:489-494.
- Holmes, J. D. (2015). "Wind Loading of Structures." 3rd Edition, CRC Press, Taylor & Francis
- Group, Boca Raton, FL.
- Huang, P., Quan, Y., and Gu, M. (2013). "Experimental Study of Aerodynamic Damping of
- Typical Tall Buildings." Hindawi Publishing Corporation, Mathematical Problems in Engi-
- neering, Volume 2013, Article ID 731572.
- 866 International Electrotechnical Commission (IEC) 60826. (2017). "Design criteria of overhead
- transmission lines." Geneva, Switzerland.
- 868 Irwin, P. A. (1977). "Wind Tunnel and Analytical Investigations of the Response of Lions' Gate
- Bridge to a Turbulent Wind." National Research Council of Canada, NAE Report LTR-LA-
- 870 210.
- 871 Irwin, P. A. (1979). "Cross-Spectra of Turbulence Velocities in Isotropic Turbulence." Journal of
- Boundary Layer Meteorology, 16, pp.337-343.
- 873 Irwin, P. A. (1992). "Full aeroelastic model tests." Aerodynamics of Large Bridges, A. Larsen
- 874 (ed.), Balkema, Rotterdam.
- 875 Irwin, P. A. (1996). "Buffeting Analysis of Long-Span Bridges." RWDI Technical Reference
- 876 Document, RD1-1996.

- 877 Isyumov, N. (1972). "Wind Tunnel Methods for Evaluating Wind Effects on Buildings and
- 878 Structures." International Symposium on Experimental Mechanics, The University of Water-
- loo, Waterloo, June 12-16.
- Jeary, A. P. (1986). "Damping in tall buildings: a mechanism and a predictor." Earthquake Engineering and Structural Dynamics, Vol. 14, 733-750.
- Jeary, A. P. (1992). "Establishing non-linear damping characteristics of structures from non-stationary response time histories." The Structural Engineer, Vol. 70, No. 4, 61-66.
- Kalaga, S., and Yenumula, P. (2017). "Design of Electrical Transmission Lines Structures and Foundations." CRC Press, Volume 1, Taylor & Francis Group, London, UK.
- Liang, S., Zou, L., Wang, D. and Cao, H. (2015). "Investigation on wind tunnel tests of a full aeroelastic model of electrical transmission tower-line system." Engineering Structures, Vol. 85, pp. 63-72.
- Lin, W. E., Savory, E., McIntyre, R. P., Vandelaar, C. S., and King, J. P. C. (2011). "A single-span aeroelastic model of an overhead electrical power transmission line with guyed lattice towers." 13th International Conference on Wind Engineering, Amsterdam.
- Lin, W. E., Savory, E., McIntyre, R. P., Vandelaar, C. S. and King, J. P. C. (2012). "The response of an overhead electrical power transmission line to two types of wind forcing". Journal of Wind Engineering and Industrial Aerodynamics, 102, 48-60.
- Loredo-Souza, A. M. (1996). "The Behaviour of Transmission Lines Under High Winds." University of Western Ontario (UWO) Digital Theses, 2650.
- Loredo-Souza, A.M. (2014). "The aeroelastic wind tunnel modeling of transmission lines and their behavior under severe boundary layer winds." Proceedings of the 9th International Conference on Structural Dynamics, EURODYN 2014, Porto, Portugal, 30 June – 2 July.
- Loredo-Souza, A. M., and Davenport, A. G. (2001). "A novel approach for wind tunnel modelling of transmission line." Journal of Wind Engineering and Industrial Aerodynamics, 89, 1017-1029.
- Loredo-Souza, A. M., and Davenport, A. G. (2003). "The influence of the design methodology in
 the response of transmission towers to wind loading." Journal of Wind Engineering and Industrial Aerodynamics, 91, 995-1005.
- Lou, W. J., Sun, B. N., and Tang, J. C. (2000). "Aeroelastic Model Investigation and Spectral Analysis of a Tall Lattice Tower." Advances in Structural Engineering, 3(2):119-30.
- Lou, W. J., Wang, X., and Jiang, Y. (2009). "Wind-Induced Responses of a High-Rise Transmission Tower to Thunderstorm Downbursts." The Seventh Asia-Pacific Conference on Wind Engineering, Nov. 8-12, Taipei, Taiwan.
- Mara, T. G., Galsworthy J. K., and Savory, E. (2010). "Assessment of vertical wind loads on lattice frame-work with application to thunderstorm winds." Wind and Structures, Vol. 13,
- 913 no.5, pp. 413-431.

- Mara, T. G. and Hong, H. P. (2013). "Effect of wind direction on the response and capacity surface of a transmission tower." Engineering Structures, 57, 493-501.
- 916 Marukawa, H., Kato, N., Fujii, K., and Tamura, Y. (1996). "Experimental evaluation of aerody-
- namic damping of tall buildings." Journal of Wind Engineering and Industrial Aerodynamics,
- 918 59, 2-3, 177-190.
- Mevada, H., and Patel, D. (2016). "Experimental determination of structural damping of differ-
- ent materials." Proceedings of the 12th International Conference on Vibration problems
- 921 (ICOVP2015), 144, pp. 100-115.
- National Oceanic and Atmospheric Administration (NOAA) (2019). "Hurricane Michael." Na-
- tional Hurricane Center Tropical Cyclone Report, AL142018.
- 924 SAP2000 Version 22.0.0 (2020), Structural Analysis Program, Computers and Structures, Inc.,
- 925 <u>www.csiamerica.com</u>
- 926 Sarkar, P. P. (1992). "New-Identification Methods Applied to the Response of Flexible Bridges
- to Wind." PhD Thesis, The John Hopkins University, Baltimore, MD.
- 928 Sarkar, P. P., Jones, N. P., and Scanlan, R. H. (1994). "Identification of Aeroelastic Parameters
- of Flexible Bridges." ASCE Journal of Engineering Mechanics, 120(8), pp. 1718-1742.
- 930 Savory, E., Parke, G. A. R., Zeinoddini, M., Toy, N., and Disney, P. (2001). "Modelling of tor-
- nado and microburst-induced wind loading and failure of a lattice transmission tower." Engi-
- 932 neering Structures, 23, 365-375.
- 933 Shehata, A. Y., and El Damatty, A. A. (2008). "Failure analysis of a transmission tower during a
- microburst." Wind and Structures, Vol. 11, No. 3, pp. 193-208.
- 935 Shichiri, Y. (1971). "Wind withstanding design for transmission line tower." Proceedings of the
- Third International Conference on Wind Engineering (3ICWE), Tokyo, Japan, pp. 451-456.
- 937 Simiu, E., and Yeo, D. (2019). "Wind Effects on Structures." John Wiley & Sons, 4th Edition.
- 938 Solari, G., and Kareem, A. (1998). "On the formulation of ASCE7-95 gust effect factor." Journal
- of Wind Engineering and Industrial Aerodynamics, 77&78, 673-684.
- 940 Strelkov, S. P. (1964). "Introduction to the Theory of Vibrations." Nauka, Moscow.
- Takeuchi, M., Maeda, J., and Ishida, N. (2010). "Aerodynamic damping properties of two trans-
- mission towers estimated by combining several identification methods." Journal of Wind En-
- gineering and Industrial Aerodynamics, 98, 872-880.
- Tamura, Y., and Suganuma, S. (1996). "Evaluation of amplitude-dependent damping and natural
- frequency of buildings during strong winds." Journal of Wind Engineering and Industrial
- 946 Aerodynamics, 59, 115-130.
- Tokoro, S., Komatsu, H., Nakasu, M., Mizuguchi, K. and Kazuga, A. (2000). "A study on wake-
- galloping employing full aeroelastic twin cable model." Journal of Wind Engineering and In-
- 949 dustrial Aerodynamics, 88, 247-261.

- 950 Yang, F., and Zhang, H. (2016). "Two case studies on structural analysis of transmission towers under downburst." Wind and Structures, Vol. 22, No. 6, 685-701.
- Zhangqi, W., Zeming, S., and Wenqiang, J. (2014). "Theoretical and Experimental Research on
 Joint Slippage Effects of Lattice Angle Steel Tower." Applied Mechanics and Materials, 477 478, pp. 660-665.
- Zhu, N., Sparling, B. F., and King, J. P. C. (2011). "Comparison of aeroelastic wind tunnel tests
 and frequency domain analyses of guyed mast dynamic response." Canadian Journal of Civil Engineering, 38, 984-997.